Metabolic constraints on growth explain how developmental temperature scales synaptic connectivity relevant for behavior.

Züfle P.[1], Batista L. L.[1], Brandão S.C., D'Uva G., Daniel C., Martelli C.*
Johannes Gutenberg University, Mainz, Germany

[1]Equal contribution
*Correspondence: cmartell@uni-mainz.de

Summary
Environmental temperature dictates the developmental pace of poikilothermic animals, but it remains unclear whether this has consequences for brain wiring and function. In *Drosophila* temperature scales synaptic connectivity in the visual system, yet the underlying reasons for such scaling, the generality of this scaling across neural circuits, and the functional implications for behavior are not understood. Here we combine anatomical, functional, and theoretical approaches to gain insights into the nature and consequences of temperature dependent synaptic scaling within the fly olfactory pathway. We show that synaptic scaling leads to heterogeneous functional effects in different olfactory subcircuits, with striking consequences for odor-driven behaviors. A first-principle model that imposes different metabolic constraints on the neural system and organism development explains these findings, and generalizes to predict brain wiring under ecologically relevant temperature cycles. Our data argue that metabolic constraints dictate the extent of synaptic scaling within neural subcircuit and that the resulting circuit architecture and function are contingent upon the availability of synaptic partners. This complex interplay between synaptic scaling and partner availability underscores the intricate impact of temperature-dependent developmental plasticity on the behavior of poikilothermic animals.

Keywords
Drosophila, developmental plasticity, temperature, olfaction

Introduction
The wiring of the nervous system follows a complex genetic plan during development. However, due to stochastic processes and environmental factors, genetically identical individuals seldomly show the same phenotypic outcome. Temperature is the environmental factor with the broadest effects in biology, as it determines the rates of all biophysical reactions of an organism (Gillooly et al., 2001). In poikilothermic animals, such as insects, worms, fish, amphibians, and reptiles, temperature determines the speed of development. Elegant ecological theories have shown that developmental times scale exponentially with temperature due to a constraint imposed by the rate limiting metabolic reaction (Gillooly et al., 2002). The development of the nervous system is certainly not exempted by the effects of temperature. However, whether a different developmental speed leads to the same wiring of the brain remains unclear.

It has been widely reported that development at different temperatures correlates with variation in behavioral phenotypes with examples in amphibians (Ohmer et al., 2023), reptiles (Abayarathna & Webb, 2020; de Jong et al., 2022; Noble et al., 2018), bees (Becher et al., 2009; Tautz et al., 2003), ants (Weidenmüller et al., 2009), and fruit flies (Baleba et al., 2023; Wang et al., 2007), Moreover, social insects as bees and ants invest a large amount of resources to keep their broods at the correct temperature throughout daily and seasonal cycles. Even small variations in developmental temperature can affect learning in bees (Zhu et al., 2023) and affect the synaptic organization of key brain areas for learning (Falibene et al., 2016; Groh et al., 2004; Wang et al., 2007). Therefore, temperature does not just determine the speed, but also the outcome of development, although the mechanistic bases of these different phenotypes are largely unknown.
A recent study in *Drosophila* reported that the number of synaptic connections in neurons of the visual system inversely correlate to temperature, i.e. when flies develop at lower temperature these neurons make more synapses and have more postsynaptic partners (Kiral et al., 2021). This leads to the question whether synaptic scaling occurs similarly throughout the brain and what consequences it has on neural computations and behavior. Answering these questions is key not only to predict the consequences of temperature changes on animal behavior in the wild, but also to fully understand the organization of the developmental program of poikilothermic animals.

Here we investigate the effects of temperature on the development and function of the olfactory system in *Drosophila*. Olfaction mediates key behaviors in animals, including foraging and mating, and it plays a major role in the organization of animal societies. Similarly to vertebrates and other insects, fruit flies express specific odorant receptors (ORs) in single Olfactory Receptor Neurons (ORNs) that project their axons into specific glomeruli of the antennal lobe (AL, equivalent of the vertebrate olfactory bulb)(Vosshall & Stocker, 2007; Wilson & Mainen, 2006). ORNs synapse onto both Local Neurons (LNs), that modulate odor representations within the AL, and Projection Neurons (PNs), that send odor information to higher brain areas. The circuit organization of this sensory pathways has been fully reconstructed and annotated from electron microscopy (EM) data (Bates et al., 2020; Schlegel et al., 2021). About half of the PNs in *Drosophila* are uniglomerular (uPNs) and therefore encode odor stimuli preserving the organization of the sensory inputs (Jeanne et al., 2018). The remaining PNs are multiglomerular (mPNs) and therefore pool information from multiple chemosensory pathways to modulate downstream circuits (Liang et al., 2013; Parnas et al., 2013; Shimizu & Stopfer, 2017; Strutz et al., 2014). uPNs and most mPNs target the Lateral Horn (LH), a multisensory area that drives innate behavior (Schultzhaus et al., 2017).

To dissect the logic behind the temperature dependency of brain wiring, we ask whether the organization and function of the olfactory system is robust to changes in developmental temperature. We use genetically encoded tools for transsynaptic labeling to quantify wiring variations across flies developed at different temperatures. We show that a general scaling with temperature of synaptic connectivity occurs also in the olfactory pathway, and we demonstrate that different synaptic partners are recruited in different subcircuits. Despite a general scaling of input activity from ORNs, odor representations are robust to changes in developmental temperature in output uPNs, likely through the corresponding scaling in local inhibition. However, the recruitment of mPNs and the differential wiring of uPNs to the LH, lead to striking differences in odor driven behavior in flies that developed at different

temperatures. Finally, we show that similarly to developmental time, synaptic scaling follows an exponential law consistent with the existence of different rate limiting metabolic reactions in the development of different neural sub-circuits.

Results

Lower temperature leads to more functional synaptic connections in one olfactory subcircuit.

We set out to investigate the effect of developmental temperature on the wiring of the olfactory system. We first analyzed neurons post-synaptic to or42b-ORNs, i.e ORNs that express the odorant receptor or42b and target the glomerulus DM1 in the AL, using trans-Tango (Talay et al., 2017), a genetic tool for transsynaptic labeling (Fig.1A). For this, flies developed at either 18ºC or 25ºC between the larval stage L2 and the end of pupal development (which we name P-100% as the time depends on temperature). Flies were then kept at 25ºC for 10 days. Strikingly more postsynaptic neurons are labeled in flies that developed at 18ºC, as suggested by denser innervations in both the AL and LH (Fig.1B-C). We quantified these differences by counting the cell bodies of the postsynaptic cells in each fly, which were more than double at 18ºC as compared to 25ºC (Fig. 1D-E). The number of postsynaptic partners reported by trans-Tango at 25ºC is largely consistent with the most connected neurons to or42b-ORNs identified in the hemibrain connectome (Scheffer et al., 2020; Schlegel et al., 2021) (Fig. 1F red bar, see Methods), while development at 18ºC seems to recruit additional neurons which are targeted sporadically by those ORNs at 25ºC (Fig. 1F).

To demonstrate that the anatomically labelled postsynaptic neurons are functionally connected to the ORNs, we modified the trans-Tango experiment to express a calcium reporter (GCaMP6s) in post-synaptic neurons, while expressing CsChrimson in the or42b-ORNs (Fig.1G). This allowed us to activate optogenetically the specific ORN type and test response in their postsynaptic partners. Electrophysiological experiments indicate that optogenetic activation of ORNs drives less activity than odors (not shown), but sufficient to induce postsynaptic neuronal responses in a dose-dependent manner (Fig.1H). Calcium transients measured within the DM1 glomerulus mostly report activity from the single uPN (which is the neuron receiving most of the ORN synapses) and did not differ at the two temperatures (Fig. 1I). However, activation in the rest of the AL is higher in flies developed at 18ºC (Fig. 1H,J), which is consistent with a larger number of multiglomerular neurons in the AL being activated. Moreover, activity is stronger in the medio-lateral AL track (mlALT) which is more strongly labeled in flies developed at 18ºC (Fig. 1K,L). We conclude that trans-Tango labels neurons that are functionally connected to the or42b-ORNs in both developmental temperatures.

More connected neurons could result from a different distribution of synapses across postsynaptic partners or from an increase in synapse number. To distinguish between these two cases, we stained the presynaptic protein Bruchpilot (Brp)(Wagh et al., 2006). We expressed a GFP tagged Brp^{Short} in the or42b-ORNs to label all its presynapses and stained the endogenous Brp (nc82, Fig. 1M). The or42b-ORNs presynaptic volume defined by the Brp^{Short} mask was consistent across the two developmental temperatures. However, flies developed at 18ºC presented higher Brp^{Short} intensity, as well as an increase in nc82-labeled Brp puncta within the presynaptic volume (Fig. 1N), together arguing for more synapses. Surprisingly, the

mean volume of Brp puncta and their intensities were also higher at 18 °C (Fig. 1O) suggesting larger active zones. The intensity and the number of synapses within the whole volume of the DM1 glomerulus, which includes connections between other neuron types, were also higher (Fig. 1O). Together, these results demonstrate that a lower developmental temperature leads both to more synapses and more synaptic partners within the DM1 glomerulus, generalizing previous observations in the visual system (Kiral et al., 2021) to the olfactory system. Here we further demonstrate that the reported synaptic partners are functionally connected to the ORNs and that synapses do not just scale in number, but also in size.

Developmental temperature differentially affects the wiring of individual glomeruli.

To get a first insight into the functional consequences of this temperature dependency, we next investigated the identity of the neurons that are recruited as postsynaptic partners at lower temperature. To do so, we extended the trans-Tango experiment to other ORNs and performed a more detailed analysis of the variable postsynaptic partners. Except for the ORNs – that have cell bodies in the antennae – AL neurons have their cell bodies distributed in four cell clusters (Fig. 2A) (Sakuma et al., 2014). The DM1 glomerulus is innervated by a single uPN located in the lateral cluster, therefore increased connectivity most likely involves multi-glomerular neurons (Fig. 1H-K). Or42b-ORNs increased connections more with neurons of the ventral and ventrolateral clusters, than other clusters (Fig. 2A). The ventral and ventrolateral cluster hosts cell bodies of 66.6% of the AL mPNs (Bates et al., 2020) and a large population of inhibitory mPNs (Liang et al., 2013; Parnas et al., 2013; Shimizu & Stopfer, 2017; Strutz et al., 2014), suggesting that Or42b-ORNs more strongly drive this population of neurons when flies develop at 18°C, consistently with imaging in the mlALT (Fig.1K). On the contrary, within the glomeruli DL5 and DL1 the corresponding ORNs increase connectivity more strongly with neurons of the lateral cluster (Fig. 2B-C). This cluster contains a large population of LNs, and mPNs mostly of unknown function (Lin et al., 2012).

We postulate that while the temperature dependent scaling of connectivity should be similar across ORN types, the identity of synaptic partners recruited will depend on available neurons in the relevant glomerulus volume. In support of these hypotheses, we found an almost identical fold change in number of synaptic partners across glomeruli (Fig. 2D). This is consistent with a similar distribution of synaptic connections across synaptic partners in these glomeruli, quantified from hemibrain EM data (Fig. 2E). This analysis shows that if all connections are scaled up or down by temperature, the relative changes would be similar across glomeruli, supporting our observation. Moreover, EM data confirm that more mPNs innervate the DM1 glomerulus than the DL1 or DL5 glomeruli, where we find instead a larger percentage of LNs (Fig. 2F).

These findings suggest different functional consequences of developmental temperature in different glomeruli. Specifically, we predict a stronger recruitment of local inhibition in all glomeruli at lower temperatures. For the DM1 glomerulus, we predict it drives stronger activity in inhibitory mPNs that send axons to the LH through the mlALT. Silencing of inhibitory mPNs from the ventral cluster has been shown to drastically reduce approach behavior to appetitive cues (Strutz et al., 2014) therefore the observe structural changes have potential functional consequences downstream of the AL.

Homeostatic compensation of temperature dependent pre-synaptic activity preserves odor coding in the AL.

To understand the consequences of altered wiring for odor coding, we evaluated both ORNs and uPNs responses to odors. Extracellular recordings from single sensilla showed that or42b-ORN transduction currents (Fig. 3A) and firing rates (Fig. 3B) elicited by odor stimuli do not differ in flies developed at different temperatures. Similar results were obtained for or59b-ORNs, innervating glomerulus DM4 (Fig. 3C-D). Moreover, within the antenna, the number of cell bodies labeled by the or-specific GAL4 line did not differ at the two temperatures (Fig. 3E). To investigate odor induced activity in the AL, we expressed the calcium sensor GCaMP6f in all orco-ORNs. In flies developed at 18ºC, two of four glomeruli (DM1 and DM4) showed higher presynaptic calcium responses when compared to 25ºC (Fig. 3F). Since the number of action potentials and the number of ORNs did not differ with temperature, we conclude that larger calcium transients in these glomeruli reflect the larger number as well as the larger size of synapses being activated (Fig. 1M-O). This raises the possibility that postsynaptic uPNs that send odor information to higher brain areas might be driven more strongly. However, uPNs in all glomeruli tested responded similarly to the tested odors in flies developed at 18ºC and 25ºC (Fig. 3G). Therefore, odor representations in the output of the AL are robust to changes in developmental temperature. Taken our anatomical analysis into account, the likely recruitment of more inhibitory local neurons appears to act as a mechanism to control for the synaptic scaling induced by developmental temperature, both presynaptically in glomeruli DL1 and DL5 and postsynaptically in DM1 and DM4, leading to robust odor representations in the uPNs of the AL.

Developmental temperature affects odor driven behavior.

We next asked whether the invariance of the uPNs' odor responses with respect to developmental temperature implies invariance in odor driven behavior. We tested the odor response of individual, 10-day old flies tethered to walk on a spherical treadmill (Fig. 4A). Contrary to our expectations, both the smell of vinegar (Fig. 4B,C) and 2-butanone (Fig. 4D-E) elicited on average a stronger increase in walking speed in flies that developed at 18ºC. These odor responses were highly reproducible across repetitions of the stimulus (Fig. 4C,E left), but very variable across individuals (Fig. 4C,E right). A stringent statistical test did not give a significant P-value for the vinegar experiment (Fig. 4B), possibly because this set of flies showed very high basal walking speed limiting the maximum delta change in response to the odor. Basal walking speed was in general larger for flies developed at 18 ºC (Fig. 4B',D'). A higher basal walking speed does not justify a higher response, rather the opposite, as flies that walk faster in this assay might not be able to reach a change in speed as high as flies that walk slower (Fig. 4B,B' and D,D'). This effect on basal walking speed is different from what was found in a previous study (Kiral et al., 2021), suggesting that basal walking speed is dependent on the behavioral task flies are subjected to.

To investigate how broadly odor-driven behaviors are affected, we tested flies in a free-walking assay where we tracked their positions while they explored a large circular arena hiding an odor source (Fig. 4F). Flies raised at both developmental temperatures visited the odor source more frequently than in the no-odor controls (Fig. 4G,H), but at any time more flies raised at 18ºC visited the odor source than flies raised at 25ºC, and spent more time at the odor in total (Fig. 4I). Similar results were obtained with 2-butanone (Fig. 4J) and for a higher testing temperature (Fig. 4K,L), in the latest case with smaller effects consistent with the spherical

treadmill (Fig. 4A-E). An analysis of walking speed in control experiments with no odor (Fig. 4M,N) demonstrates that during active times, the flies' walking speed is mostly determined by testing temperature, while developmental temperature mostly affects the activity level, quantified as the probability to find the flies active. Since at both testing temperatures, the activity levels of flies developed at 18ºC are higher, we conclude that the higher odor occupancy of these flies is not due to inactivity or poor locomotion. We conclude that independently of possible effects on the motor system, flies developed at lower temperatures are more attracted to vinegar and 2-butanone.

Developmental temperature shapes connectivity patterns between glomeruli and lateral horn neurons.

Since the output activity of the AL measured in uPNs was invariant to developmental temperature (Fig. 3), we postulated that the different behavioral phenotypes should result from differences downstream of the AL. Innate odor preference is determined by the wiring of uPNs onto LH neurons (Schultzhaus et al., 2017) and modulated by mPNs (Liang et al., 2013; Parnas et al., 2013; Shimizu & Stopfer, 2017; Strutz et al., 2014). We have already shown that ORNs recruit more mPNs when developing at 18ºC (Fig. 2), specifically in the DM1 glomerulus that responds to 2-butanone and vinegar (Fig. 3). Moreover, larger calcium transients were measured in the medial lateral antennal lobe tract (mlALT) upon optogenetic activation of DM1-ORNs, which contains mostly mPNs (Tanaka et al., 2012)(Fig. 1K). Therefore, we set out to check if the connections of uPNs onto LHNs were also altered by developmental temperature. We labeled the glomeruli connected to a specific LHN type, PD2a1/b1, using the genetically encoded retrograde tracer BAcTrace (Cachero et al., 2020) (Fig. 5A). Differently from trans-Tango, this genetic tool only labels presynaptic partners from defined cell types, in this case uPNs (and 3 mPNs, targeted by *VT033006-LexA*). Although the innervation of uPNs' axons into the LH have been shown to be stereotypic across individuals (Jefferis et al., 2007), we found a large degree of inter-individual variation and asymmetry in connectivity across hemispheres (Fig. 5B) as previously reported (Cachero et al., 2020). Developmental temperature did not increase the number of uPNs connected to PD2a1/b1 neurons (Fig. 5G), but determined which glomeruli were more often connected to these neurons in a population of individuals (Fig. 5E,F). While DL1, DL3 and DL4 were similarly connected in the two conditions, the probability to find VM2 and VM3 connected is much lower in flies developed at 18ºC (Fig. 5H). Overall, there is a change in the type of glomeruli that PD2a1/b1 receives inputs from. The connectivity quantified in EM data is consistent with the variation found using BAcTrace (Fig. 5D,E,I), with small discrepancies that could be explained by the different genetic background and by a weaker labeling of specific glomeruli (as DM1) by the *VT033006-LexA* line used, as also discussed in (Cachero et al., 2020). Overall, we conclude that developmental temperature significantly shifts the wiring pattern of uPNs to the LH.

The BAcTrace approach reveals a similar number of connected uPNs to PD2a1/b1, but this analysis is restricted to a specific cell type. We therefore used another genetically encoded retrograde tracer, retro-Tango (Sorkaç et al., 2023), to label all the presynaptic partners of PD2a1/b1 (Fig. 5K). The number of PD2a1/b1 neurons labeled at the two temperatures did not differ (Fig. 5K). However, we find similar asymmetric labeling of the glomeruli as with BAcTrace (Fig. 5K, not quantified) and a larger number of presynaptic neurons with cell bodies in the AL clusters, with larger effects in the ventral cluster that contains mPNs (Fig. 5M). This

increase in the number of synaptic partners is consistent with a general scaling of connectivity with temperature throughout the brain.

PD2a1/b1 neurons mediate approach to appetitive cues and are specifically required for preference to vinegar (Dolan 2018). However, activation of PD2a1/b1 is not sufficient to drive behavior (M. J. Dolan et al., 2019), suggesting that the differential wiring of the PNs on this LHN is unlikely the sole explanation for the behavioral differences we observed (Fig. 4). We expect that the wiring of other LHNs to uPNs is also affected and that together with the differential recruitment of mPNs this leads to the temperature dependency of odor driven behavior.

Scaling laws of synaptic partners and developmental times

Finally, we asked how synaptic connectivity scales across a wider range of temperatures. *Drosophila melanogaster* lives in different climates, with a thermal range between 11 and 32°C (Pétavy et al., 1997). We used trans-Tango to characterize connectivity patterns of the or42b-ORNs in flies that developed at the extreme temperatures (12-32°C). These conditions are highly stressful, and if persistent, female reproduction success would go to zero (Trotta et al., 2006). However, the temperature shift in our experiments was applied only between L2 and P+100%, and the flies that eclosed were viable for at least 10 days. Flies that developed at 12°C established a large number of synaptic partners, including neurons that target regions outside the canonical olfactory pathway (Fig. 6A). Importantly, the anatomy of the ORNs is strongly affected at this temperature, showing axonal extensions protruding radially from the DM1 glomerulus (Fig. 6C, compare to 6E) as well as strong mistargeting to a more anterior glomerulus, VA2 (Fig. 6D). Flies developed at 31°C instead show very few neurons connected to DM1, much fewer than animals raised at 25°C (Fig. 6B), including the uPN, mPNs and LNs in variable number across individual brains (not shown).
Across all developmental temperatures tested, the number of ORNs remained constant (Fig. 6H), but the number of synaptic partners scaled exponentially with temperature (Fig. 6F-G), similarly to the scaling of developmental time (Fig. 6I). We reasoned that the scaling of these two factors, number of synaptic partners and developmental time, could derive from similar first principles. Gillooly et al. have proposed that the rate of development scales with temperature proportionally to the Boltzmann factor of the rate limiting metabolic reaction (Gillooly et al., 2002). Assuming that flies eclose to a similar mass across temperatures, developmental time should scale like $\frac{t}{t_0} = e^{-\frac{E}{KT_a^2}(T-T_0)}$ (see Methods), where t_0 is the developmental time at a reference temperature T_0 (here $T_0 = 25°\mathrm{C}$), E is highest activation energy in the metabolism (corresponding to the slowest reaction), K is the Boltzmann constant, T_a is the absolute zero. In our experiments, we found $\alpha = \frac{E}{KT_a^2} = 0.11 \pm 0.02$ (fig. 6G) in agreement with estimates in other animals (Gillooly et al., 2002). We reasoned that if the development of the neural circuit would be limited by the same reaction rate, then development should result in the same brain connectivity. If, otherwise, the development of the neural system is limited by a reaction with lower activation energy E', it should scale with Boltzmann factor $e^{-\frac{E'}{KT}}$ with $E' < E$; the neural circuit of interest will therefore develop (form synapses) at its own pace, but for an amount of time that is determined by the whole organism, therefore leading to a larger number of synapses. To calculate the fold change in connectivity, we assume that axonal growth and synaptogenesis scale with a ζ=¾ power law:

$\frac{dn}{dt} \sim an^{\frac{3}{4}}$, as for body mass (Gillooly et al., 2002). Many biological processes, including growth, scale allometrically with the ¾ law (Feldman & McMahon, 1983; Peters, 1983) a phenomenological observation that has received a first principles explanation based on the fractal nature of the distribution of nutrients and resources in a 3D volume by a space -filling network of branching tubes (West et al., 1997, 1999). Given the tree-like structure of axons, along which mitochondria and proteins need to be transported, and of other energy supplier in the brain (trachea, glia), the ¾ law is a reasonable assumption for the growth of the neural system. From these assumptions, it is possible to derive an analytical function for the scaling of synaptic connectivity with temperature: $\frac{n}{n_0} = e^{-4\frac{E-E\prime}{KT_a^2}(T-T_0)}$ (see Methods). When $\Delta E = 0$, the same number of connections are established across temperatures. For $\Delta E > 0$, there will be a difference in connectivity determined by the parameter $\beta = \frac{4\Delta E}{KT_a^2}$. β can be smaller or larger than the scaling factor for the developmental time, α. In the olfactory circuit we find $\beta = 0.12(\pm 0.01) > \alpha$. In the visual system Kiral et al. reported a fold change $\frac{n_{18}}{n_0}$~1.5 which would correspond to $\beta < \alpha$. Therefore, the model is consistent with the different scaling values observed in different subcircuits.

To test the validity of the model, we asked what happens in more ecological relevant conditions when flies develop on diurnal temperature cycles. Does development result in the same wiring outcome as for flies developed the mean temperature? We set flies to grow on ecologically realistic temperature cycles with the same mean temperature (24°C) but different amplitudes (20-28°C and 16-32°C, Fig. 6J). These conditions lead to different phenotypes, with more synaptic partners in 20-28°C cycles than 16-32°C cycles, both significantly different from the 25°C condition (Fig. 6K). We further show that the temperature experienced after eclosion does not strongly affect connectivity (Fig. 6K). We therefore asked whether the growth model fitted above would be consistent with these findings. Integrating the growth rate over temperature cycles (see Methods) and using the estimate for α and β from the fixed temperature experiments (Fig. 6G,I), we were able to predict the number of synaptic partners for the cycling temperature protocol (Fig. 6L), and specifically a higher number of synaptic partners for cycles with lower amplitude. The model further predicts that circuit connectivity scales inversely with the amplitude ΔT of the temperature cycle as: $\frac{\tilde{n}}{\bar{n}} = \left(\frac{\cosh(\gamma\Delta T)}{\cosh(\alpha\Delta T)}\right)^4$, always leading to less connections than at the mean temperature $\bar{T}$.

We conclude that the circuit specificity of temperature-dependent synaptic scaling is consistent with a growth model with different rate limiting metabolic reactions for the whole organisms and for the specific neural sub-circuits.

Discussion

The development of a whole organism requires the parallel and coordinated growth of mass and, in the brain, the establishment of functional synaptic connectivity in different subcircuits. Developmental programs are highly temporally structured, but in poikilothermic animals developmental speed depends on external temperature. Previous work has demonstrated that developmental temperature scales synaptic connectivity in the fly visual system and predicted that robustness to this environmental perturbation should be found in the functional output of a scalable wiring program (Kiral et al., 2021). Combining anatomical and physiological approaches, we demonstrate that scalable microcircuits of different composition within distinct glomeruli mediate the robust encoding of odor stimuli in the AL. However,

downstream of the AL, the different convergence of odor information onto LH neurons leads to temperature-dependent behavioral outcomes in individual animals. Our data is consistent with a growth model with different rate limiting reactions for different subcircuits, which predicts the scaling of wiring in cycling temperature conditions. We propose that circuit intrinsic metabolic constraints lead to differential effects of temperature on the development of the nervous system and we provide evidence that network connectivity strongly depends on the availability of synaptic partners.

Mechanisms for robust function in a synaptically enriched circuit.

The analysis of neural connectivity of distinct glomeruli reveals two important consequences of temperature. First, an overall increase in synaptic partners corresponds to a larger number and larger size of synapses (Brp enriched). This synaptic scaling is consistent with the larger calcium transients measured in some of the glomeruli in ORNs axons (Fig. 3F). However, within all glomeruli a larger number of LNs would be recruited at lower temperatures, likely driving higher inhibitory feedbacks. The balance between excitation and inhibition is key for the function of healthy brains and there is evidence that this balance is achieved developmentally during synapse formation (Cline, 2005). In sensory systems, lateral inhibition sets the operational set point for stimulus encoding through a divisive normalization (Heeger, 1992; Olsen et al., 2010). In the fly olfactory system, GABAergic inhibition is distributed at both pre- and post-synapses in ORN-uPN connections (Olsen & Wilson, 2008; Root et al., 2008), in agreement with our observation that in some glomeruli calcium transients are already compensated at the ORN axon terminals, while in others, odor response is fully robust only after the first synaptic connection (Fig. 3). However, it remains unclear whether the scaling of inhibition is the sole mechanism that keeps responses temperature invariant. It is possible that the presynaptic scaling is also a homeostatic response to weaker post-synapses (Böhme et al., 2019; Frank et al., 2020). Overall, we conclude that the peripheral olfactory system is designed to compensate the temperature driven synaptic scaling and to keep odor information invariant to developmental temperature shifts.

Mechanisms for the modulation of odor preference within the LH.

Despite the robust odor representations within the AL, behavioral response to appetitive odor cues is strongly affected by developmental temperature in two different assays (Fig. 6). Innate odor preference arises in the LH where uPNs target LHNs within a rather complex wiring logic (M. J. Dolan et al., 2019b; Jeanne et al., 2018). Our analysis demonstrates that LHNs necessary for attraction to vinegar (M.-J. J. Dolan et al., 2018) receive temperature dependent odor information from the antennal lobe through the differential wiring of uPNs (Fig. 5). The quantified temperature dependency of synaptic connectivity between uPNs and PD2a1/b1 is only a lower bound, as the lexA line that labels uPNs just covers about half of the glomeruli. Furthermore, variation in uPNs-PD2a1/b1 connections is unlikely the only explanation for the behavioral differences. First, the connectivity of other LHNs is also likely affected by temperature with possible synergistic and redundant control of behavior. Second, at lower temperatures, the wiring of the ORNs within the AL recruits mPNs that target the LH and the protocerebrum. The function of this large population of neurons (>50% of the total number of PNs) is still unclear, from which about half of them are predicted to be GABAergic (Bates et al., 2020). GABAergic mPNs have modulatory effects on preference and discrimination (Liang et al., 2013; Parnas et al., 2013; Strutz et al., 2014). Importantly, silencing inhibitory mPNs reduces approach towards appetitive odors (Strutz et al., 2014). The other half of mPNs is

predicted to be cholinergic and their contribution to downstream odor processing or behavior is unknown. Investigating the function of mPNs will be key to understand what consequences their recruitment at lower temperatures could have on behavior.

Metabolic constraints to the development of the neural system.

As previously proposed by Kiral et al., an increased number of synapses at lower temperature is the result of a difference between the scaling of circuit development and the scaling of animal growth rates. Here we show that fly developmental times scale exponentially in agreement with proposed theories that assume a metabolic constraint to growth rate. We extended this theoretical framework to model the rate of synapse formation. To do so, we made two assumptions. The first is that a different rate limiting reaction constraints neural development and that this might vary across subcircuits. This agrees with the finding of different scaling parameters in the visual and olfactory system and does not exclude that other subcircuits might develop at rates consistent with the rest of the organism, and therefore no synaptic scaling should be observed. This argument could explain why in bees, just 1ºC difference in temperatures leads to a lower synaptic output from the olfactory but not the visual pathway into the mushroom body (Groh et al., 2004).
The second assumption we made is that neural/synaptic growth scales with the fractional power ζ=3/4, a parameter derived from geometrical considerations on the fractal nature of the distributions of resources throughout capillaries, rather than volumetrically (West et al., 1999). Our data at fixed temperature are consistent with any $\zeta<1$, but developmental outcome measured in presence of fluctuating temperatures is well predicted by a ¾ exponent (West et al., 2001) (Fig. 6). The highly plausible assumptions, the success of the model in explaining our data and the compatibility with observations in another sensory circuit (Kiral et al., 2021), suggest that similar principles may apply to other circuits and organisms.

Phenotypic variation and constrained pathways

Overall, our study suggests that phenotypic variation should be variably expected upon a temperature shift during development because of different metabolic constraints on growth imposed on different neural subcircuits. Moreover, synaptic scaling recruits partners based on their spatio-temporal availability. Clearly some connections in the brain are critical for survival and these are probably evolved to wire no matter the temperature. Experiments done at extremely high temperatures reveal the backbone of the olfactory pathway, i.e. the wiring of ORNs onto a single uPN, a few mPNs and LNs. Studying these extreme conditions might reveal insights on evolutionary constrains on circuit design.
The brain has evolved many strategies to keep circuits' function robust to environmental factors (Haddad & Marder, 2018; Marder et al., 2014). But while such robustness holds true within some subcircuits (individual glomeruli in our study), it cannot be assumed to occur throughout the brain, in our case in the downstream pathways to the LH. In addition, we observe surprisingly variable connectivity of LH neurons in individuals developed at the same temperature. In the future, it will be necessary to determine how much of this variation is biological to establish a link to idiosyncratic behavior (K. Honegger & de Bivort, 2018; K. S. Honegger et al., 2020). Nonetheless our study raises the question of whether variation itself, stochastic or environmental, is an evolutionary selected feature and whether the stochastic and environmental factors are or are not independent from each other. We suggest that understanding the evolutionary relevance of non-genetic wiring variation in the brain of

poikilothermic animals will require to consider environmental temperature as a key determinant of brain structure and function.

Acknowledgment

We thank Marion Silies for access to resources, Marion Silies, Filippo Calzolari and Sebastian Cachero for critical reading of the manuscript, Christopher Schnaitmann for help with *in vivo* imaging, Luisa F. Ramirez Ochoa for discussions of the model, Constantin Müller, Nancy Benjamin and Polina Krasnova for help with behavioral experiments, the biology workshop at JGU for developing the behavioral assay, Christoph Rickert for help with confocal imaging, Maria Ioannidou, Tristan Walter, Fritz Francisco and Angela Albi for help with video tracking, Sebastian Cachero and Greg Jefferis for sharing a new BAcTrace construct, David Deutsch for materials for the spherical treadmill, Robin Hiesinger, Carsten Duch, Bassem Hassan, members of the FOR5289 and members of the Silies lab for discussions. We further thank Sabine Schmitt, Simone Renner and Jonas Chojetzki for technical and administrative support.

Author contribution

P.Z., L.B. and C.M. designed the study. P.Z. and L.B. performed and analyzed the anatomical experiments, L.B., S.C.B. and G.D.U. performed and analyzed *in vivo* calcium imaging, G.D.U., C.D. and S.C.B. set up, performed, and analyzed behavioral experiments, C.M. performed electrophysiology, analyzed data, developed the model, C.M. and L.B. wrote the manuscript and all authors edited it. This work was supported by the DFG grants MA7804/2-1 and MA7804/3-1 to C.M.

Declaration of interests

The authors declare no competing interests.

Figures

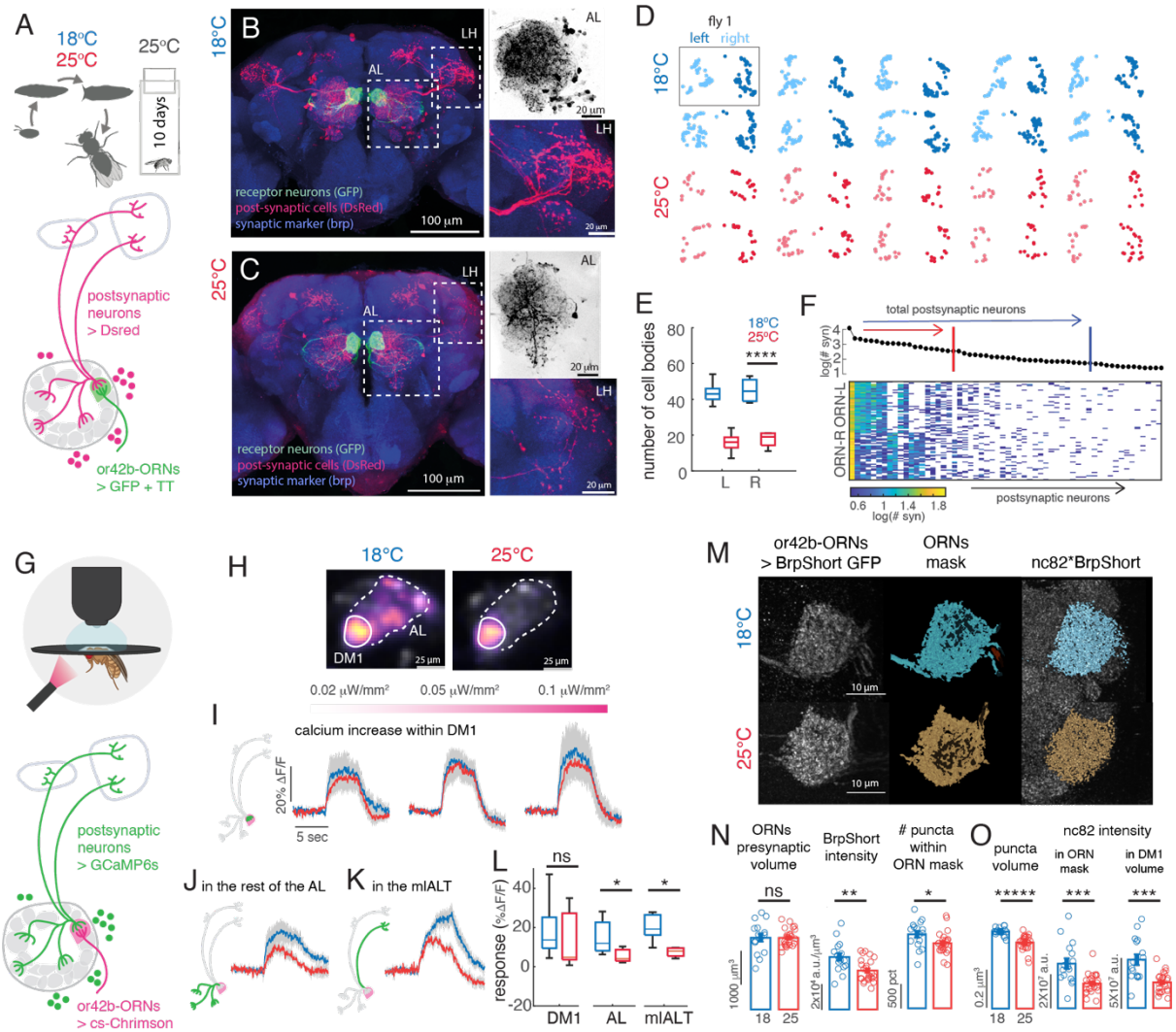

Figure 1. Developmental temperature determines ORN synaptic partners in a glomerulus. A) Flies expressing the trans-Tango construct under control of or42b-Gal4 were placed at 25°C or 18°C between L2 and P+100% and then dissected when 10 days old. Or42b-ORNs send its axons in the DM1 glomerulus where they target both local neurons (LNs) and projection neurons (PNs) that send their axons to higher brain regions. **B-C)** Example brains from flies developed at the two temperatures. Immunostaining labels ORNs that express GFP (green), post-synaptic partners expressing dsRed (red) and all synapses through anti-Brp (nc82, blue). Insets are close-ups of the innervations in the AL (dsRed signal only shown in grey scale) and LH. **D)** Cell body locations in left (L) and right (R) hemisphere of each individual fly. **E)** Boxplot showing median and quartiles of the number of postsynaptic partners, Kruskal-Wallis test, $p < 10^{-7}$, n=10. **F)** Connectivity matrix from hemibrain EM data: right hemisphere postsynaptic partners of DM1-ORNs from both hemispheres. Post-synaptic partners on the x-axis are ranked by the total number of input synapses from these ORNs, as quantified above. Color scale indicates the number of synapses in log scale. The red and blue bar indicate the mean number of postsynaptic partners counted within one hemisphere in the trans-Tango experiment. **G)** Schematics of the experiment where the usual trans-Tango reporter dsRed was replaced by GCaMP6s, and activity of presynaptic neurons is induced by CsChrimson. **H)**

Example responses for flies developed at different temperatures. Color bar indicates ΔF/F calculated for each pixel. White lines indicate the region of interests (roi) used for quantification. **I)** Mean optogenetic response quantified in the DM1 glomerulus for three stimulus intensities. **J)** Optogenetic response to 0.05μW/mm^2 quantified in the rest of the AL and **K)** in the mlALT. **L)** Boxplot showing median, quartiles and min/max response taken as the mean in 9s following stimulus onset. Significant differences were observed in the AL roi (Kruskal-Wallis test, p=0.02, n=4-7) and in the mlALT (Kruska-Wallis test, p=0.01, n=4-7). **M)** Left to right: Brp[Short]-GFP fluorescence expressed in or42b-ORNs, 3D mask reconstructed from it, nc82 staining of synaptic puncta and 3D reconstruction of the puncta within the ORN mask for the two temperatures. **N)** Volume, mean intensity and number of puncta within the Brp[Short]-mask and **O)** puncta volume and intensity within the ORN mask and within the whole glomerulus volume (error bars indicate SEM, n = 16 hemibrains at 18 °C and n = 25 at 25 °C, Kruskal-Wallis test, *p<0.05, **p<10^{-2}, ***p<10^{-3}, *****p<10^{-5}).

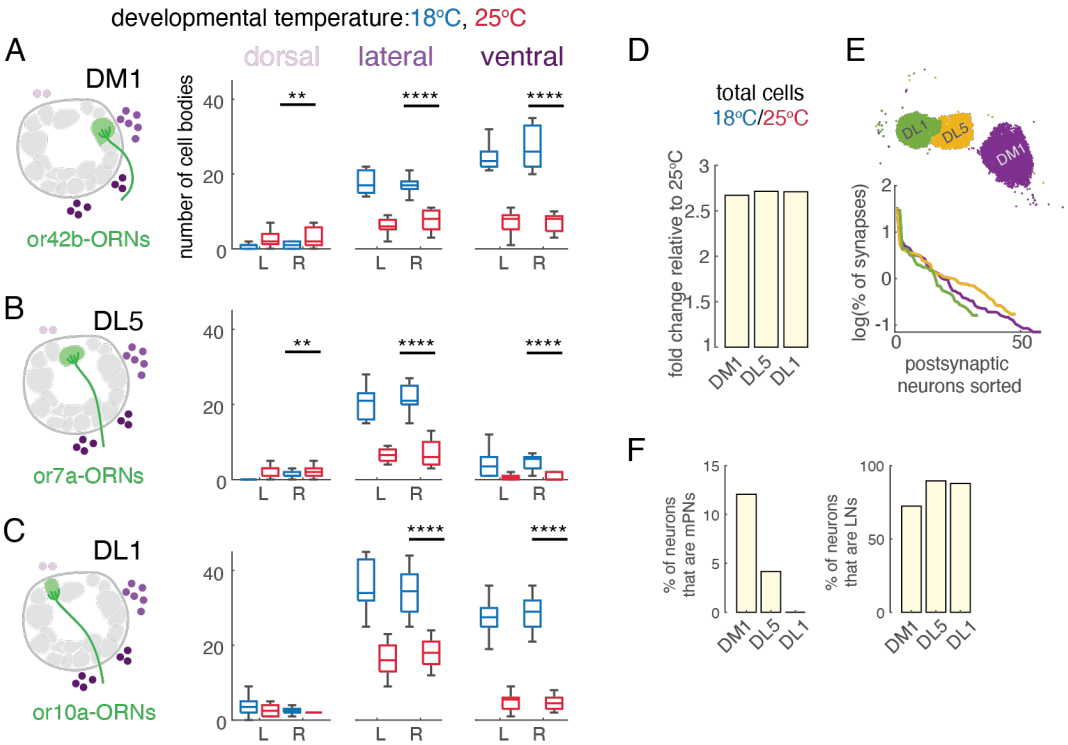

Figure 2. Differential effects of temperature on wiring and wiring variability. A-C) Trans-Tango analysis of connectivity of three different ORNs. Number of synaptic partners in different cell clusters of the AL, showing a differential increase across glomeruli. Boxplots indicate median and quartiles, whiskers indicate maximum and minimum values. Sample size at 18/25 °C: DM1 n=20/23, DL5 n=10/10, DL1 n=10/10, Kruskal-Wallis test *p<0.05, **p<10^{-2}, ***p<10^{-3}, *****p<10^{-5} **D)** Fold change in number of synaptic partners relative to 25°C. **E)** Allocation of ORN output synapses onto individual synaptic partners for the three glomeruli, as quantified from EM data (Hemibrain). The number of synapses was normalized to the total for each ORN class. Postsynaptic neurons are sorted based on the number of synaptic inputs they receive. Top: spatial location of the synapses analyzed (only right hemisphere). **F)** Percentage of postsynaptic neurons annotated in the Hemibrain dataset as mPNs and LNs.

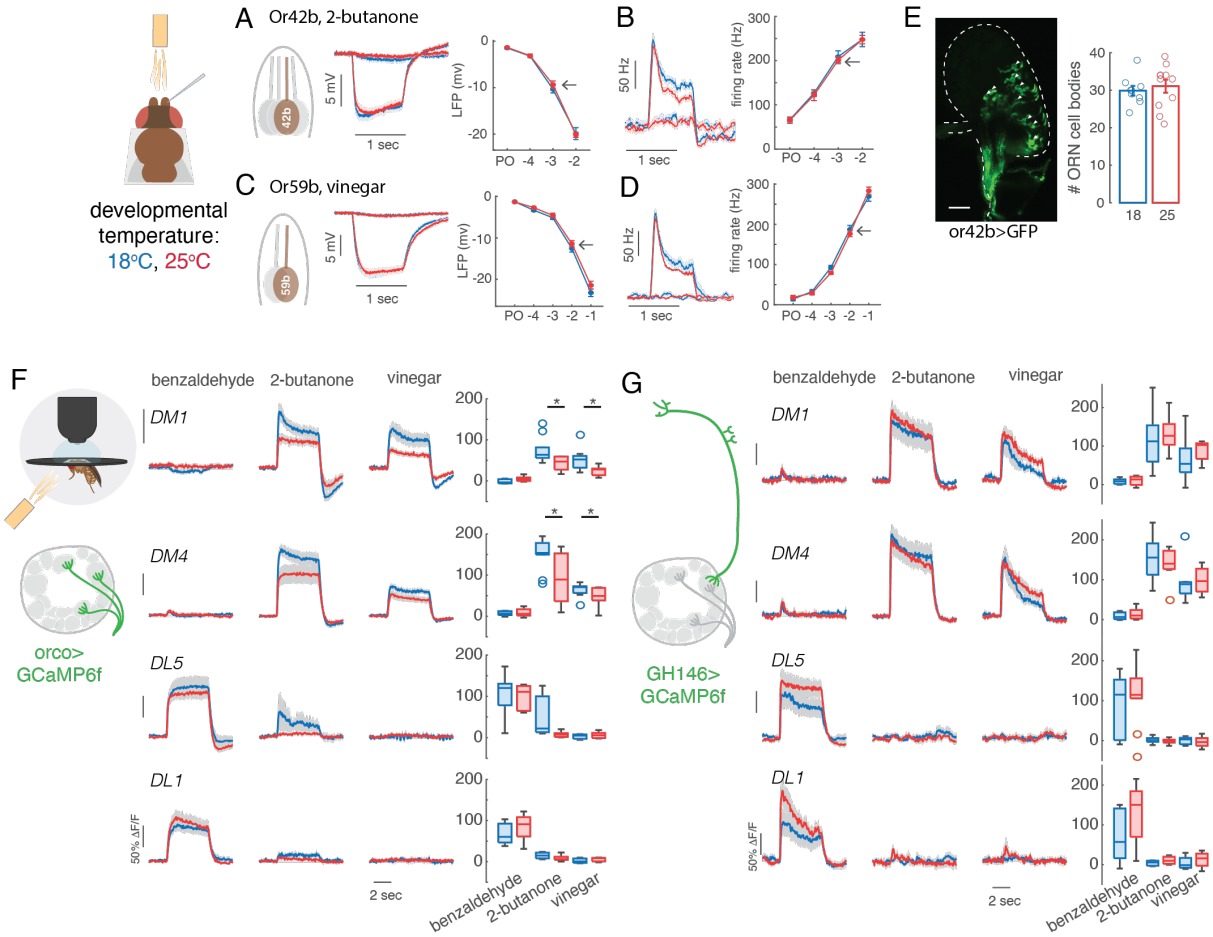

Figure 3. Scaling and normalization of odor responses in input and output neurons of the AL. A) Left to right: Single sensillum recordings from the ab1 sensillum containing a single or42b-ORN. Mean response of the LFP to a 1s pulse of 2-butanone at 10^{-3} dilution and Paraffin Oil (PO) control. Amplitude of the LFP calculated as the maximum drop for each odor concentration. **B)** Firing rate response to a 1s pulse of 2-butanone at 10^{-3} dilution and PO control calculated in 100ms sliding window. Right: mean peak response for each concentration tested. **C-D)** Same as **A-B** for the ab2 sensillum containing one or59b-ORN. **E)** Confocal image of the antenna showing GFP expression in or42b-ORNs. Bar plot indicates mean and SEM, individual data points are overlayed. **F)** Calcium imaging from the ORN axon terminals in the AL, quantified within 3 glomeruli for flies developed at the different temperatures. Boxplot indicates median and quartiles of the response, whiskers indicate min/max responses. **G)** Same as **F**, but the calcium reporter was expressed in uPNs and responses were quantified in the dendritic arborizations within corresponding AL glomeruli. Shaded areas indicate SEM, boxplots indicate median, quartile and min/max values, n=5-10 depending on the glomerulus-odor combination.

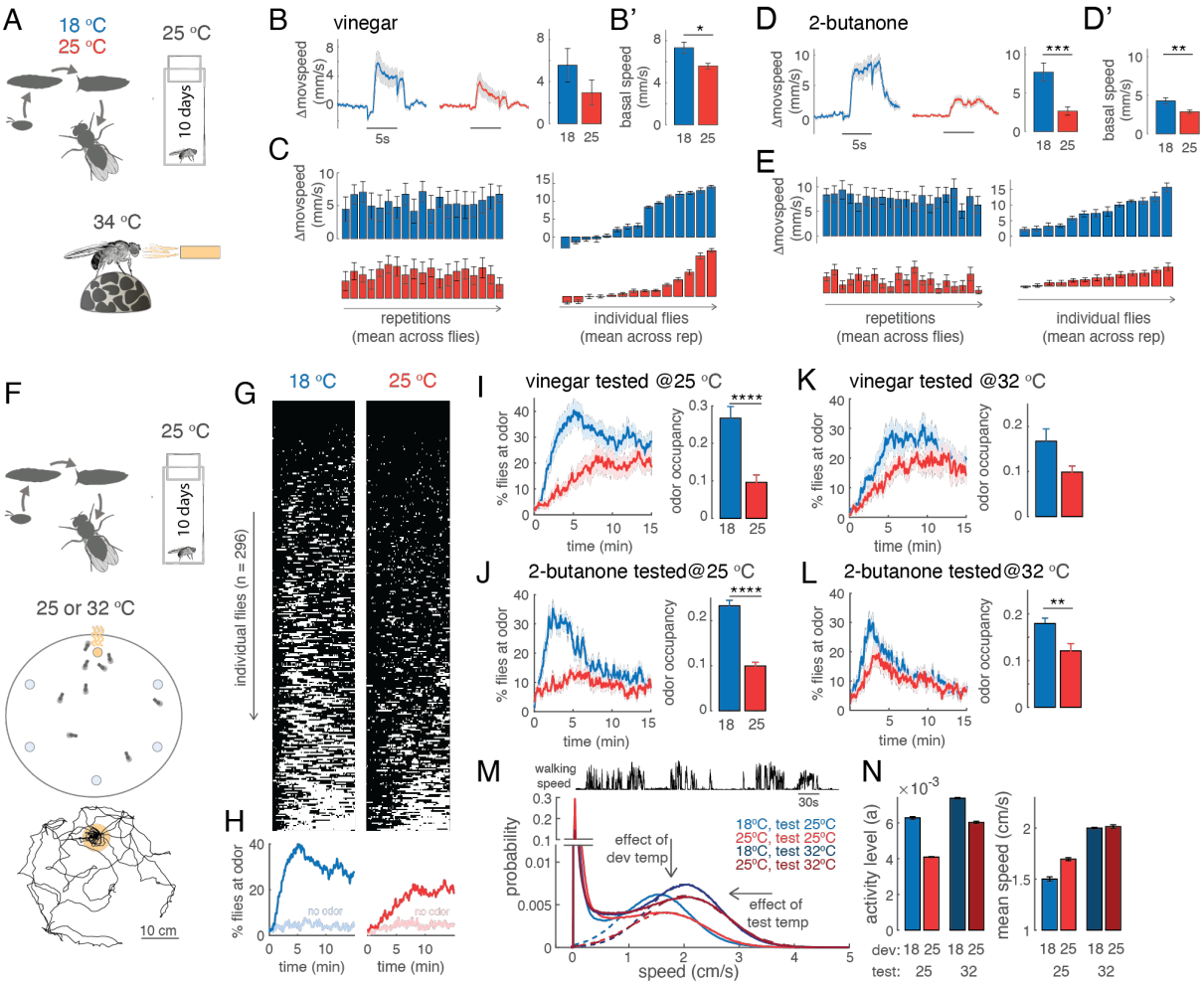

Figure 4. Developmental temperature affects odor-driven behavior. A) Flies were placed at 25°C (red) or 18°C (blue) between L2 and P+100% and otherwise kept at 25°C. When 10 days old, odor response was tested at 34°C on a spherical treadmill setup (see Methods). **B)** Odor response calculated as change in moving speed as a function of time in response to 5s stimulation (Δmovspeed = speed-basal speed); bar plot: mean change in moving speed within the first 2s of stimulation (p =0.1, n=14,13). **B')** Basal walking speed is estimated within 3s before stimulus onset (p = 0.02). **C)** Mean response to each consecutive stimuli repetitions averaged across all flies (right), and mean response of each individual fly across repetitions, showing large variation across individuals (left). **D-E)** Same as **B-C** for a second set of flies tested with 2-butatone ($p<10^{-3}$, n=13,13). **F)** Top: Same breeding protocol as in A, but odor preference was tested at either 25°C or 32°C in a free walking assay. Middle: Circular arena of 40 cm radius with an odor source randomly placed in one of six possible locations. Bottom: Sample trajectory of one fly tracked for 15 min (see Methods). **G)** Binary maps showing individual flies located at the odor source (<5 cm, white) as a function of time and **H)** percentage of flies at the odor (vinegar). An empty odor vial was used as control in an independent set of experiments (shaded curves). **I)** Average percentage of flies at the odor source and odor occupancy (bar plot). Shaded area and error bars indicate SEM. Odor occupancy calculated as the integral under the curve in the first 7 minutes, being 1 if all flies spend 100% of the time at the odor ($p<10^{-4}$, n=21,20). **J)** Same as **I** for the odor 2-butanone ($p<10^{-6}$, n=19,20). **K-L)** Same as **I-J** but for a testing temperature of 32 °C, for vinegar (p=0.09, n=19,18) and 2-butanone (p=0.006, n=20,20). **M)** Top: example of walking speed for one fly,

showing bouts of activity. Bottom: probability of walking speed calculated from all data (flies and times) of each condition, showing a bimodal distribution with a large peak in zero that represents inactive flies; dotted lines indicate gaussian fit $ae^{-\left(\frac{x-b}{c}\right)^2}$ to the active flies. **N)** Parameter estimates from the gaussian fit: the amplitude of the gaussian (a) as an estimate of the activity levels (probability to be active), and the mean (b) and an estimate of the mean walking speed during active times. Error bars indicate confidence intervals on the fitted parameters.

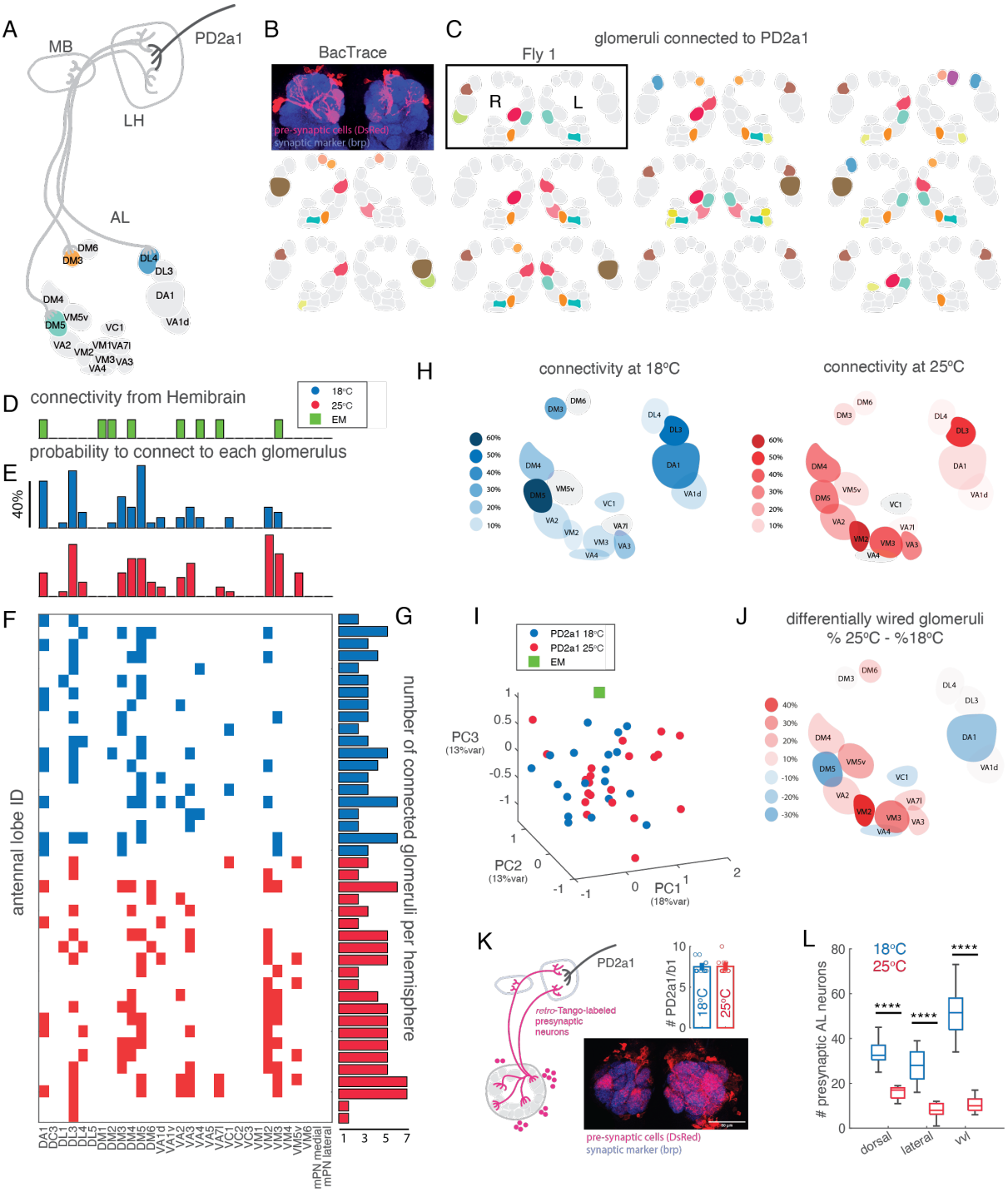

Figure 5. Temperature dependent wiring of uPNs into the LH. A) Schematics of the BAcTrace experiment, showing the neurons PD2a1/b1 and candidate pre-synaptic uPNs from the AL. **B)** Confocal image of a sample brain showing labeled uPNs arborizations in the AL. **C)** Binary connectivity patterns of the glomeruli to PD2a1/b1 in 11 brains from flies developed at 25°C. Each glomerulus is marked in the same color across flies. **D)** Binary connectivity pattern quantified from EM data for the glomeruli considered. **E)** Probability to find a certain glomerulus connected to PD2a1/b1 for each temperature. **F)** Binary connectivity map quantified in individual hemibrains (y-axis) to glomeruli (x-axis); n=20,22. **G)** Number of connected glomeruli in each hemisphere. **H)** Connectivity patterns at 18°C (blue) or 25 °C (red). The shaded colors indicate the probability to find the glomerulus connected (same as in **E**). **I)** PCA of combined data shows connectivity of individual hemibrains for both temperature conditions and EM data. **J)** Glomeruli more often connected in flies that developed at 25°C (red) or 18°C (blue), calculated as the difference of the data in **H**. **K)** Schematics of the retro-Tango experiment starting from PD2a1/b1, bar plot showing mean number of PD2a1/b1 neurons labeled by the split-Gal4 line (errorbars are SEM, n=12,11 hemibrains) and a sample confocal image of the AL, showing innervated glomeruli. **L)** Boxplot showing median, quartiles and min/max values for the number of PD2a1/b1 presynaptic partners from three cell clusters; vvl includes cell bodies in the ventral and ventro-lateral cluster ($p<10^{-4}$, n=12,11 hemibrains).

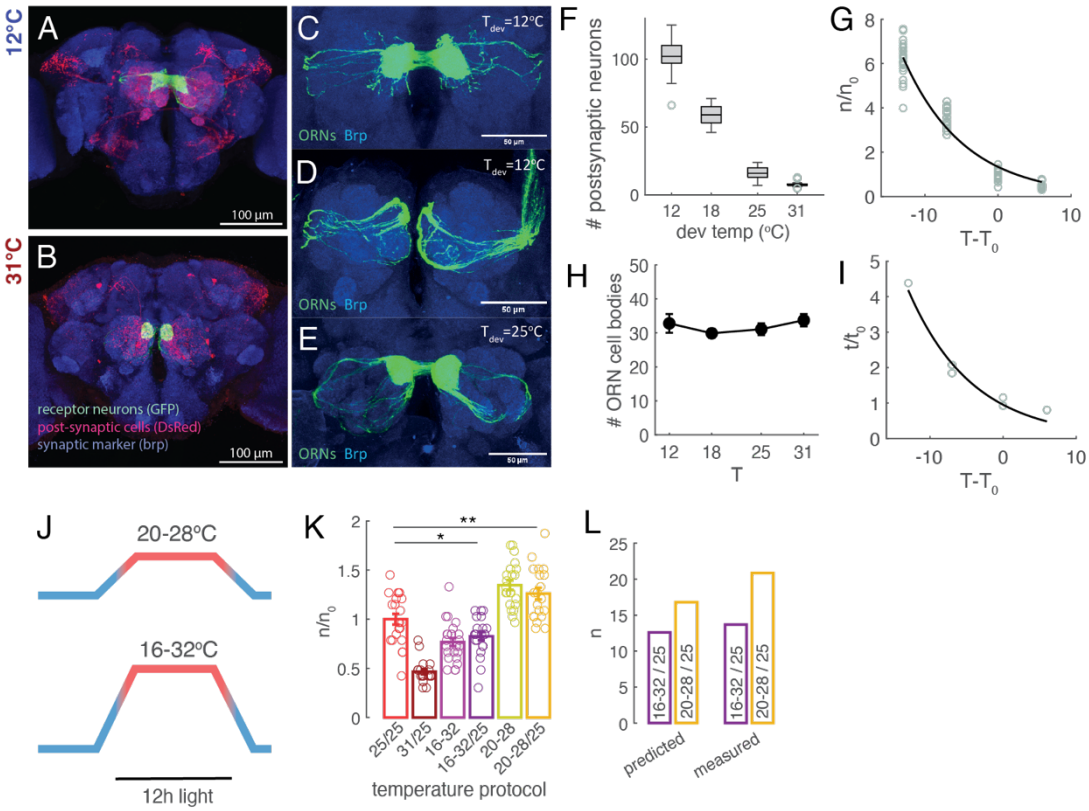

Figure 6. Scaling law for network connectivity. A-B) Example brains of flies expressing trans-Tango under control of or42b-Gal4 and developed at 12°C or 31°C. **C-E)** Magnification of ORN axons labeled by GFP. **C)** Or42b-ORNs mistargeting outside the DM1 glomerulus in flies that developed at 12°C. **D)** Same fly as in **C** imaged at a more anterior focal plane, showing innervations of the or42b-ORNs in the glomerulus VA2. **E)** Normal axonal projections in flies

developed at 25°C. **F)** Box plot of the number of postsynaptic partners as a function of developmental temperature. **G)** Single data points as in **F**, normalized by the mean number of neurons connected at a reference temperature (25°C) and plotted as a function of the difference from the reference temperature. The line indicates the exponential fit. **H)** Mean number of ORNs cell bodies as a function of temperature (error bars indicate SEM). **I)** Fold change in developmental time with respect to the temperature difference from 25°C and exponential fit. **J)** Schematics of the temperature and light cycles. **K)** Fold change in synaptic partners from 25°C for all temperature protocols. Temperature shifts were applied only between L2 and P-100% then flies were moved to 25°C, except for the light-purple and light-yellow bars for which flies were kept through adulthood at the cycling temperatures. **L)** Predicted (see Methods) and measured (same data as in **K**) numbers of post-synaptic partners in temperature cycles.

References

Abayarathna, T., & Webb, J. K. (2020). Effects of incubation temperatures on learning abilities of hatchling velvet geckos. *Animal Cognition*, *23*(4), 613–620. https://doi.org/10.1007/S10071-020-01365-4

Baleba, S. B. S., Mahadevan, V. P., Knaden, M., & Hansson, B. S. (2023). Temperature-dependent modulation of odor-dependent behavior in three drosophilid fly species of differing thermal preference. *Communications Biology 2023 6:1*, *6*(1), 1–11. https://doi.org/10.1038/s42003-023-05280-5

Bates, A. S., Schlegel, P., Roberts, R. J. V., Drummond, N., Tamimi, I. F. M., Turnbull, R., Zhao, X., Marin, E. C., Popovici, P. D., Dhawan, S., Jamasb, A., Javier, A., Serratosa Capdevila, L., Li, F., Rubin, G. M., Waddell, S., Bock, D. D., Costa, M., & Jefferis, G. S. X. E. (2020). Complete Connectomic Reconstruction of Olfactory Projection Neurons in the Fly Brain. *Current Biology*, *30*(16), 3183-3199.e6. https://doi.org/10.1016/j.cub.2020.06.042

Becher, M. A., Scharpenberg, H., & Moritz, R. F. A. (2009). Pupal developmental temperature and behavioral specialization of honeybee workers (Apis mellifera L.). *Journal of Comparative Physiology. A, Neuroethology, Sensory, Neural, and Behavioral Physiology*, *195*(7), 673–679. https://doi.org/10.1007/S00359-009-0442-7

Böhme, M. A., McCarthy, A. W., Grasskamp, A. T., Beuschel, C. B., Goel, P., Jusyte, M., Laber, D., Huang, S., Rey, U., Petzoldt, A. G., Lehmann, M., Göttfert, F., Haghighi, P., Hell, S. W., Owald, D., Dickman, D., Sigrist, S. J., & Walter, A. M. (2019). Rapid active zone remodeling consolidates presynaptic potentiation. *Nature Communications 2019 10:1*, *10*(1), 1–16. https://doi.org/10.1038/s41467-019-08977-6

Cachero, S., Gkantia, M., Bates, A. S., Frechter, S., Blackie, L., McCarthy, A., Sutcliffe, B., Strano, A., Aso, Y., & Jefferis, G. S. X. E. (2020). BAcTrace, a tool for retrograde tracing of neuronal circuits in Drosophila. *Nature Methods*. https://doi.org/10.1038/s41592-020-00989-1

Cline, H. (2005). Synaptogenesis: A balancing act between excitation and inhibition. *Current Biology*, *15*(6), R203–R205. https://doi.org/10.1016/j.cub.2005.03.010

de Jong, M., Phillips, B. L., Llewelyn, J., Chapple, D. G., & Wong, B. B. M. (2022). Effects of developmental environment on animal personality in a tropical skink. *Behavioral Ecology and Sociobiology*, *76*(10), 1–13. https://doi.org/10.1007/S00265-022-03240-3/TABLES/3

Dolan, M. J., Frechter, S., Bates, A. S., Dan, C., Huoviala, P., Roberts, R. J., Schlegel, P., Dhawan, S., Tabano, R., Dionne, H., Christoforou, C., Close, K., Sutcliffe, B., Giuliani, B., Li, F., Costa,

M., Ihrke, G., Meissner, G. W., Bock, D. D., … Jefferis, G. S. (2019). Neurogenetic dissection of the Drosophila lateral horn reveals major outputs, diverse behavioural functions, and interactions with the mushroom body. *ELife*. https://doi.org/10.7554/eLife.43079

Dolan, M.-J. J., Ghislain, B.-G., Bates, A. S., Frechter, S., Aurélie, L.-S.-A., Aso, Y., Roberts, R. J. V. J. V, Schlegel, P., Wong, A., Hammad, A., Bock, D., Rubin, G. M., Preat, T., Plaçais, P.-Y. Y., & Jefferis, G. S. X. E. S. X. E. (2018). Communication from Learned to Innate Olfactory Processing Centers Is Required for Memory Retrieval in Drosophila. *Neuron*, *100*(3), 651-668.e8. https://doi.org/10.1016/j.neuron.2018.08.037

Falibene, A., Roces, F., Rössler, W., & Groh, C. (2016). Daily Thermal Fluctuations Experienced by Pupae via Rhythmic Nursing Behavior Increase Numbers of Mushroom Body Microglomeruli in the Adult Ant Brain. *Frontiers in Behavioral Neuroscience*, *10*(APRIL). https://doi.org/10.3389/FNBEH.2016.00073

Feldman, H. A., & McMahon, T. A. (1983). The 3/4 mass exponent for energy metabolism is not a statistical artifact. *Respiration Physiology*, *52*(2), 149–163. https://doi.org/10.1016/0034-5687(83)90002-6

Frank, C. A., James, T. D., & Müller, M. (2020). Homeostatic control of Drosophila neuromuscular junction function. *Synapse (New York, N.y.)*, *74*(1), 22133. https://doi.org/10.1002/SYN.22133

Gillooly, J. F., Brown, J. H., West, G. B., Savage, V. M., & Charnov, E. L. (2001). Effects of size and temperature on metabolic rate. *Science (New York, N.Y.)*, *293*(5538), 2248–2251. https://doi.org/10.1126/SCIENCE.1061967

Gillooly, J. F., Charnov, E. L., West, G. B., Savage, V. M., & Brown, J. H. (2002). Effects of size and temperature on developmental time. *Nature*, *417*(6884), 70–73. https://doi.org/10.1038/417070A

Groh, C., Tautz, J., & Rössler, W. (2004). Synaptic organization in the adult honey bee brain is influenced by brood-temperature control during pupal development. *Proceedings of the National Academy of Sciences of the United States of America*, *101*(12), 4268–4273. https://doi.org/10.1073/PNAS.0400773101

Haddad, S. A., & Marder, E. (2018). Circuit Robustness to Temperature Perturbation Is Altered by Neuromodulators. *Neuron*, *100*(3), 609-623.e3. https://doi.org/10.1016/J.NEURON.2018.08.035

Heeger, D. J. (1992). Normalization of cell responses in cat striate cortex. *Visual Neuroscience*, *9*(2), 181–197. https://doi.org/10.1017/S0952523800009640

Honegger, K., & de Bivort, B. (2018). Stochasticity, individuality and behavior. *Current Biology*, *28*(1), R8–R12. https://doi.org/10.1016/j.cub.2017.11.058

Honegger, K. S., Smith, M. A. Y., Churgin, M. A., Turner, G. C., & De Bivort, B. L. (2020). Idiosyncratic neural coding and neuromodulation of olfactory individuality in Drosophila. *Proceedings of the National Academy of Sciences of the United States of America*, *117*(38), 23292–23297. https://doi.org/10.1073/pnas.1901623116

Jeanne, J. M., Fişek, M., & Wilson, R. I. (2018). The Organization of Projections from Olfactory Glomeruli onto Higher-Order Neurons. *Neuron*, *98*(6), 1198-1213.e6. https://doi.org/10.1016/J.NEURON.2018.05.011

Jefferis, G. S. X. E., Potter, C. J., Chan, A. M., Marin, E. C., Rohlfing, T., Maurer, C. R., & Luo, L. (2007). Comprehensive maps of Drosophila higher olfactory centers: spatially segregated fruit and pheromone representation. *Cell*, *128*(6), 1187–1203. https://doi.org/10.1016/J.CELL.2007.01.040

Kiral, F. R., Dutta, S. B., Linneweber, G. A., Hilgert, S., Poppa, C., Duch, C., von Kleist, M., Hassan, B. A., & Hiesinger, P. R. (2021). Brain connectivity inversely scales with developmental temperature in Drosophila. *Cell Reports*, *37*(12). https://doi.org/10.1016/J.CELREP.2021.110145

Liang, L., Li, Y., Potter, C. J., Yizhar, O., Deisseroth, K., Tsien, R. W., & Luo, L. (2013). GABAergic Projection Neurons Route Selective Olfactory Inputs to Specific Higher-Order Neurons. *Neuron*, *79*(5), 917–931. https://doi.org/10.1016/J.NEURON.2013.06.014

Lin, S., Kao, C. F., Yu, H. H., Huang, Y., & Lee, T. (2012). Lineage Analysis of Drosophila Lateral Antennal Lobe Neurons Reveals Notch-Dependent Binary Temporal Fate Decisions. *PLOS Biology*, *10*(11), e1001425. https://doi.org/10.1371/JOURNAL.PBIO.1001425

Marder, E., O'Leary, T., & Shruti, S. (2014). Neuromodulation of Circuits with Variable Parameters: Single Neurons and Small Circuits Reveal Principles of State-Dependent and Robust Neuromodulation. *Https://Doi.Org/10.1146/Annurev-Neuro-071013-013958*, *37*, 329–346. https://doi.org/10.1146/ANNUREV-NEURO-071013-013958

Noble, D. W. A., Stenhouse, V., & Schwanz, L. E. (2018). Developmental temperatures and phenotypic plasticity in reptiles: a systematic review and meta-analysis. *Biological Reviews*, *93*(1), 72–97. https://doi.org/10.1111/BRV.12333

Ohmer, M. E. B., Hammond, T. T., Switzer, S., Wantman, T., Bednark, J. G., Paciotta, E., Coscia, J., & Richards-Zawacki, C. L. (2023). Developmental environment has lasting effects on amphibian post-metamorphic behavior and thermal physiology. *Journal of Experimental Biology*, *226*(9). https://doi.org/10.1242/JEB.244883/306975/AM/DEVELOPMENTAL-ENVIRONMENT-HAS-LASTING-EFFECTS-ON

Olsen, S. R., Bhandawat, V., & Wilson, R. I. (2010). Divisive normalization in olfactory population codes. *Neuron*, *66*(2), 287–299. https://doi.org/10.1016/j.neuron.2010.04.009

Olsen, S. R., & Wilson, R. I. (2008). Lateral presynaptic inhibition mediates gain control in an olfactory circuit. *Nature*, *452*(7190), 956–960. https://doi.org/10.1038/nature06864

Parnas, M., Lin, A. C., Huetteroth, W., & Miesenböck, G. (2013). Odor Discrimination in Drosophila: From Neural Population Codes to Behavior. *Neuron*, *79*(5), 932–944. https://doi.org/10.1016/J.NEURON.2013.08.006

Pétavy, G., Morin, J. P., Moreteau, B., & David, J. R. (1997). Growth temperature and phenotypic plasticity in two Drosophila sibling species: probable adaptive changes in flight capacities. *Journal of Evolutionary Biology*, *10*(6), 875–887. https://doi.org/10.1111/J.1420-9101.1997.TB00003.X

Peters, R. H. (1983). The Ecological Implications of Body Size. *The Ecological Implications of Body Size*. https://doi.org/10.1017/CBO9780511608551

Root, C. M., Masuyama, K., Green, D. S., Enell, L. E., Nässel, D. R., Lee, C.-H., & Wang, J. W. (2008). A presynaptic gain control mechanism fine-tunes olfactory behavior. *Neuron*, *59*(2), 311–321. https://doi.org/10.1016/j.neuron.2008.07.003

Sakuma, C., Anzo, M., Miura, M., & Chihara, T. (2014). Development of olfactory projection neuron dendrites that contribute to wiring specificity of the Drosophila olfactory circuit. *Genes & Genetic Systems*, *89*(1), 17–26. https://doi.org/10.1266/GGS.89.17

Scheffer, L. K., Xu, C. S., Januszewski, M., Lu, Z., Takemura, S. Y., Hayworth, K. J., Huang, G. B., Shinomiya, K., Maitin-Shepard, J., Berg, S., Clements, J., Hubbard, P. M., Katz, W. T., Umayam, L., Zhao, T., Ackerman, D., Blakely, T., Bogovic, J., Dolafi, T., … Plaza, S. M. (2020). A connectome and analysis of the adult drosophila central brain. *ELife*, *9*, 1–74. https://doi.org/10.7554/ELIFE.57443

Schlegel, P., Bates, A. S., Stürner, T., Jagannathan, S. R., Drummond, N., Hsu, J., Capdevila, L. S., Javier, A., Marin, E. C., Barth-Maron, A., Tamimi, I. F. M., Li, F., Rubin, G. M., Plaza, S. M., Costa, M., & Jefferis, G. S. X. E. (2021). Information flow, cell types and stereotypy in a full olfactory connectome. *ELife*, *10*. https://doi.org/10.7554/ELIFE.66018

Schultzhaus, J. N., Saleem, S., Iftikhar, H., & Carney, G. E. (2017). The role of the Drosophila lateral horn in olfactory information processing and behavioral response. *Journal of Insect Physiology*, *98*, 29–37. https://doi.org/10.1016/J.JINSPHYS.2016.11.007

Shimizu, K., & Stopfer, M. (2017). A Population of Projection Neurons that Inhibits the Lateral Horn but Excites the Antennal Lobe through Chemical Synapses in Drosophila. *Frontiers in Neural Circuits*, *11*. https://doi.org/10.3389/FNCIR.2017.00030

Sorkaç, A., Moșneanu, R. A., Crown, A. M., Savaş, D., Okoro, A. M., Memiş, E., Talay, M., & Barnea, G. (2023). retro-Tango enables versatile retrograde circuit tracing in Drosophila. *ELife*, *12*. https://doi.org/10.7554/ELIFE.85041

Strutz, A., Soelter, J., Baschwitz, A., Farhan, A., Grabe, V., Rybak, J., Knaden, M., Schmuker, M., Hansson, B. S., & Sachse, S. (2014). Decoding odor quality and intensity in the Drosophila brain. *ELife*, *3*, e04147. https://doi.org/10.7554/ELIFE.04147

Talay, M., Richman, E. B., Snell, N. J., Hartmann, G. G., Fisher, J. D., Sorkaç, A., Santoyo, J. F., Chou-Freed, C., Nair, N., Johnson, M., Szymanski, J. R., & Barnea, G. (2017). Transsynaptic Mapping of Second-Order Taste Neurons in Flies by trans-Tango. *Neuron*, *96*(4), 783-795.e4. https://doi.org/10.1016/J.NEURON.2017.10.011

Tanaka, N. K., Endo, K., & Ito, K. (2012). Organization of antennal lobe-associated neurons in adult Drosophila melanogaster brain. *Journal of Comparative Neurology*, *520*(18), 4067–4130. https://doi.org/10.1002/cne.23142

Tautz, J., Maier, S., Groh, C., Rössler, W., & Brockmann, A. (2003). Behavioral performance in adult honey bees is influenced by the temperature experienced during their pupal development. *Proceedings of the National Academy of Sciences of the United States of America*, *100*(12), 7343–7347. https://doi.org/10.1073/PNAS.1232346100/ASSET/27B1EDC6-15C9-4F50-ABE7-873CC8626106/ASSETS/GRAPHIC/PQ1232346002.JPEG

Trotta, V., Calboli, F. C. F., Ziosi, M., Guerra, D., Pezzoli, M. C., David, J. R., & Cavicchi, S. (2006). Thermal plasticity in Drosophila melanogaster: A comparison of geographic populations. *BMC Evolutionary Biology*, *6*(1), 1–13. https://doi.org/10.1186/1471-2148-6-67/TABLES/4

Vosshall, L. B., & Stocker, R. F. (2007). Molecular architecture of smell and taste in Drosophila. *Annual Review of Neuroscience*, *30*, 505–533. https://doi.org/10.1146/ANNUREV.NEURO.30.051606.094306

Wagh, D. A., Rasse, T. M., Asan, E., Hofbauer, A., Schwenkert, I., Dürrbeck, H., Buchner, S., Dabauvalle, M. C., Schmidt, M., Qin, G., Wichmann, C., Kittel, R., Sigrist, S. J., & Buchner, E. (2006). Bruchpilot, a protein with homology to ELKS/CAST, is required for structural integrity and function of synaptic active zones in Drosophila. *Neuron*, *49*(6), 833–844. https://doi.org/10.1016/J.NEURON.2006.02.008

Wang, X., Green, D. S., Roberts, S. P., & de Belle, J. S. (2007). Thermal disruption of mushroom body development and odor learning in Drosophila. *PloS One*, *2*(11). https://doi.org/10.1371/JOURNAL.PONE.0001125

Weidenmüller, A., Mayr, C., Kleineidam, C. J., & Roces, F. (2009). Preimaginal and adult experience modulates the thermal response behavior of ants. *Current Biology : CB*, *19*(22), 1897–1902. https://doi.org/10.1016/J.CUB.2009.08.059

West, G. B., Brown, J. H., & Enquist, B. J. (1997). A general model for the origin of allometric scaling laws in biology. *Science (New York, N.Y.)*, *276*(5309), 122–126. https://doi.org/10.1126/SCIENCE.276.5309.122

West, G. B., Brown, J. H., & Enquist, B. J. (1999). The fourth dimension of life: fractal geometry and allometric scaling of organisms. *Science (New York, N.Y.)*, *284*(5420), 1677–1679. https://doi.org/10.1126/SCIENCE.284.5420.1677

West, G. B., Brown, J. H., & Enquist, B. J. (2001). A general model for ontogenetic growth. *Nature 2001 413:6856*, *413*(6856), 628–631. https://doi.org/10.1038/35098076

Wilson, R. I., & Mainen, Z. F. (2006). Early events in olfactory processing. *Annual Review of Neuroscience*, *29*, 163–201. https://doi.org/10.1146/ANNUREV.NEURO.29.051605.112950

Zhu, C., Li, H., Xu, X., Zhou, S., Zhou, B., Li, X., Xu, H., Tian, Y., Wang, Y., Chu, Y., Zhang, X., & Zhu, X. (2023). The mushroom body development and learning ability of adult honeybees are influenced by cold exposure during their early pupal stage. *Frontiers in Physiology*, *14*, 1173808. https://doi.org/10.3389/FPHYS.2023.1173808/FULL

STAR Methods

Key resources table

REAGENT or RESOURCE	SOURCE	IDENTIFIER
Antibodies		
chicken anti-GFP	Abcam	Abcam Cat# ab13970, RRID:AB_300798
rabbit anti-DsRed	Takara Bio	Takara Bio Cat# 632496, RRID:AB_10013483
Mouse anti-nc82	deposited to the DSHB by Buchner, E.	DSHB Cat# nc82, RRID:AB_2314866
Goat anti-chicken Alexa Fluor 488	Jackson Immunoresearch	Jackson ImmunoResearch Labs Cat# 103-545-155, RRID:AB_2337390
Donkey anti-rabbit Alexa Fluor 568	Thermo Fisher Scientific	Thermo Fisher Scientific Cat# A10042, RRID:AB_2534017
Donkey anti-mouse Alexa Fluor 647	Thermo Fisher Scientific	Thermo Fisher Scientific Cat# A-31571, RRID:AB_162542
Chemicals, peptides, and recombinant proteins		
PBS	GIBCO	Art. #70011044
Paraformaldehyde	Polysciences	Art. #00380-1
Triton X-100	Roth	Art. #3051.2
Normal goat serum	Thermo Scientific	Art. #31872
VectaShield	Biozol	Art. #VEC-H-1000
Apple Cider Vinegar	Ja! REWE, Apfel Essig	N/A
2-butanone	Sigma-Aldrich Co.	Art. #34861-M, CAS 78-93-3
Benzaldehyde	Sigma-Aldrich Co.	Art. #B1334, CAS 100-52-7=
Mineral Oil	Sigma-Aldrich Co.	Art. #330779-1L, CAS 8042-47-5
All trans retinal	Sigma-Aldrich Co.	Art. #R2500
Sigmacote®	Sigma-Aldrich Co.	Art. #SL2
Experimental Models: Organisms/Strains		
D. melanogaster: UAS-brpD3::GFP	Gift from Robin Heisinger	N/A
D. melanogaster: or42b-Gal4	Bloomington Drosophila Stock Center (BDSC)	RRID: BDSC_9972
D. melanogaster: or7a-Gal4	BDSC	RRID: BSDC_23907
D. melanogaster: or10a-Gal4	BDSC	RRID: BSDC_9944
D. melanogaster: trans-Tango	BDSC	RRID: BSDC_77124
D. melanogaster: QUAS-GCamp6s; trans-Tango	BDSC	RRID: BSDC_95316
D. melanogaster: PD2a1/b1 split-Gal4 (R48F03-p65AD; R37G11-Gal4DBD)	BDSC	RRID: BSDC_86654
D. melanogaster: BacTrace (w^+,QUAS-mtdTomato_UAS-	Gift from S. Cachero	N/A

CD2(attp8); pJFRC19-Syb::GFP-P10(VK37) VT033006-LexAp65(JK22C) LexAop-minQf-noV5-minSNAP25-HIVNES-Syntaxin(VK18);P{20XUASI-B3R.PEST}attp2 pJFRC161-B3RT-B2B3RT-HBMBoNTa2xGFPnb(VK5) QUAS-mtdTomato::HA)		
D. melanogaster: GH146-Gal4	Gift from A. Fiala	N/A
D. melanogaster: orco-Gal4	BDSC	RRID: BSDC_23292
D. melanogaster: isoD1	Gift from M. Silies	N/A
D. melanogaster: UAS-GCamp6f	BDSC	RRID: BSDC_42747
D. melanogaster: UAS-CsChrimson	BDSC	RRID: BSDC_82181
D. melanogaster: retro-Tango	BDSC	RRID: BSDC_99661
Software and algorithms		
ImageJ		RRID:SCR_003070
Leica Application Suite X	Leica	RRID:SCR_013673
MATLAB	MathWorks	RRID:SCR_001622
Adobe Illustrator	Adobe	RRID:SCR_010279
Hemibrainr (v. 0.1.0)	Bates AS, Jefferis GSXE (2020)	https://github.com/natverse/hemibrainr
Pylon viewer (64-Bit, 6.3.0.10295)		
FicTrac	(Moore et al., 2014)	
Trex 1.1.8_3	(Walter & Couzin, 2021)	RRID:SCR_022361
Python 3.9.12		RRID:SCR_008394
RStudio		RRID:SCR_000432
Napari-pyclesperanto	(Haase, 2021)	

Method Details

Experimental model / Fly husbandry

Flies were raised on standard molasses-based food, at 65% humidity and on controlled 12h:12h light-dark cycle. All flies were kept at 25°C as embryos and after eclosion. Flies were placed at different temperature (12°C, 18°C, 25°C and 31°C depending on the experiment) between the second instar larva stage (L2) and the end of metamorphosis. As the time of development depends on temperature, we call the end point of metamorphosis P-100%. For optogenetics experiments, flies were kept in standard molasses-based food with 1mM all-trans retinal (Sigma-Aldrich) in the dark for ≥ 72h before experiments. In all experiments only females were used. Exact genotypes are given in the table below.

Name	Genotype	Figure
or42b > trans-Tango	w^+, UAS-myrGFP.QUAS-mtdTomato-3xHA; trans-Tango / CyO ; or42b-Gal4 / +	Figure 1B-E, Figure 2A, Figure 6
or42b > trans-Tango QUAS-Gcamp6s	w^+ 10x QUAS-Gcamp6s; trans-Tango / UAS-CsChrimson; or42b-Gal4 / +	Figure 1H-K
or42b > brpShort GFP	;+;UAS-BRP D3::GFP/or42b-Gal4	Figure 1M
or7a > trans-Tango	w^+, UAS-myrGFP.QUAS-mtdTomato-3xHA; trans-Tango / or7a-Gal4	Figure 2B
or10a > trans-Tango	w^+, UAS-myrGFP.QUAS-mtdTomato-3xHA; trans-Tango / or10a-Gal4	Figure 2C
Or42b > GFP	w^+, UAS-myrGFP.QUAS-mtdTomato-3xHA; trans-Tango / CyO ; or42b-Gal4 / +	Figure 3E
orco > GCamp6f	w^+; UAS-Gcamp6f / +; orco-Gal4 / +	Figure 3A-D,F
GH146 > GCamp6f	w^+; UAS-Gcamp6f / GH146-Gal4	Figure 3G
PD2a1/b1 > BacTrace	w^+, QUAS-mtdTomato,UAS-CD2/+; Syb::GFP, VT033006-LexAp65, LexAop-minQf-noV5-minSNAP25-HIVNES-Syntaxin/R48F03-p65AD; UASI-B3R.PEST,B3RT-B2B3RT-HBMBoNTa2xGFPnb, QUAS-mtdTomato::HA / R37G11-Gal4DBD	Figure 5B-J
PD2a1 > retro-Tango	y w^+ QUAS-mtdTomato-3xHA; retro-Tango / + ; 10xUAS-retro-Tango/ R48F03-p65AD; R37G11-Gal4DBD / +	Figure 5K-L

Temperature cycle experiment

For temperature cycle experiments flies were kept at an 12h: 12h light-dark cycle, and either a temperature cycle/protocol of 20-28°C or 16-32°C, with 8h of temperature plateau and temperature changes of 2°C/h and 4°C/h, respectively.

Immunohistochemistry and confocal

Female flies (9-11 days post eclosion) were anesthetized with ice and then briefly submersed on ethanol 70%. Flies were dissected on cold Phosphate Buffer Saline (PBS) for no longer than 20 minutes and fixated for 50 minutes in 2% paraformaldehyde (PFA, Polysciences, diluted in PBS) rotating at room temperature. All subsequent incubation and washes were done while rotating, in the dark. Brains were washed three times in PBT (PBS with 0.5 % Triton x-100, Roth) for 15 min and then blocked for one hour in 5% normal goat serum (NGS, Thermo Scientific, in 0.3 % PBT). Samples were incubated in primary antibody mixture (chicken anti-GFP 1:1000; rabbit anti-DsRed 1:500; mouse anti-nc82 1:25) for 48hrs at 4°C, then washed three times in PBT and incubated in secondary antibody mix (goat anti-chicken Alexa Fluor 488; donkey anti-rabbit Alexa Fluor 568; donkey anti-mouse Alexa Fluor 647, all at 1:200) for 48hrs at 4°C. Finally, brains were washed three times in PBT and mounted in VectaShield (Biozol) antifading medium. Brains were imaged on a Leica SP8 microscope with a 20, 40 or 63x objective depending on the experiment.

After image acquisition, the number cell bodies of postsynaptic partners were manually counted using Fiji's cell counter plugin. Cell body numbers were classified according to the position around the antennal lobe: dorsal, lateral or ventro-lateral (including both ventro-lateral and ventral clusters).

BrpShort analysis

Confocal images of individual DM1 glomeruli were processed using a custom code in python, with the package pyclesperanto (Haase, 2021). Images contained a brp-Short and nc82 channel. Both channels were pre-processed with Gaussian Blur (1.0, 1.0, 1.0) and top hat box (20.0, 20.0, 1.0). DM1-ORNs mask was made using the Brp-Short channel, by applying Voronoi Otsu Labeling and then merging the touching labels. For the whole DM1 glomerulus mask, the DM1-ORN volume was closed using the function closing labels. Single nc82 puncta were labeled by Voronoi Otsu Labeling and restricted to the DM1 glomerulus mask. Labels volume and fluorescence intensity were acquired using the statistics of labelled pixels from pyclesperanto.

In vivo calcium imaging

Flies developed at either 18°C or 25°C, 9-11 days post eclosion, were anesthetized on ice and mounted on a custom holder using UV-cured glue (Bondic). Saline solution (5mM Hepes, 130 mM NaCl, 5mM KCl, 2 mM $MgCl_2$, 2mM $CaCl_2$, 36 mM Saccharose – pH 7.3) was added. The cuticle covering the fly's head, as well as obstructing trachea, were removed.

Functional imaging was done on an Investigator two-photon microscope (Bruker) coupled to a tunable laser (Spectraphysics Insight DS+) with a 25×/1.1 water-immersion objective (Nikon). Laser excitation was tuned to 920 nm, and less than 20 mW of excitation was delivered to the specimen. Emitted light passed through a SP680 short-pass filter, a 560 lpxr dichroic filter and a 525/70 filter. PMT gain was set to 850 V. The microscope was controlled with the PrairieView (5.4) software.

Optogenetics

For optogenetic activation light from a 625 nm diode was directed using an optic fiber to the fly's antenna. The diode was controlled in flight-back mode from the imaging software, allowing simultaneous acquisition and excitation. The light stimulus protocol consisted of 5s series of light pulses, presented 5 times with intervals of 30s. Stimulus intensity in Fig. 1H was measured at the fly position with this protocol.

Odor delivery

Flies were exposed to a continuous clean air airflow (1L/min), in which either an odor stream (100mL/min) or a clean balancer airflow (100 mL/min) was redirected through a solenoid valve (LEE), so that the final airflow reaching the fly was around 1.1mL/min. For creating the gas dilutions four mass flow controllers were used (Analyt-MTC) and controlled using a custom MATLAB (MathWorks) script and an Arduino board. Odors were prepared as a liquid 5 mL 10^{-2} volumetric dilution in 20ml glass vials (2-butanone and benzaldehyde in mineral oil, apple cider vinegar in MiliQ Water). The final volumetric gas dilution used was 10^{-5}. Odor stimulation consisted of three repetitions of a 5 s, with 30 s intervals in between.

Electrophysiology

Single sensillum recordings were performed as previously described (Martelli et al., 2013) using a silver-chloride electrode and glass pipettes filled with sensillum lymph ringer. Electrical signals were amplified using an extracellular amplifier (EXT-02F-1, npi) with head stage (EXT-EH), bandpass filtered (300–5000 Hz), digitized at 20KHz using a NI board (NI-6212). Data were acquired with the matlab toolbox *kontroller* (Gorur-Shandilya et al., 2017) https://github.com/emonetlab/kontroller. Spikes were sorted using a custom MATLAB routine.

Odor delivery

Flies were exposed to a constant airflow (1L/min) and an odor stimulus was delivered by switching a 3-way solenoid valve that directed a secondary airflow (100 mL/min) through a Pasteur pipette as in (Martelli et al., 2013; Martelli & Fiala, 2019). The pipette contained a filter paper with 50µl odor dilution. Volumetric odor dilutions were prepared in either mineral oil or MiliQ Water. Stimuli were controlled by custom made software in MATLAB and arduino.

Behavioral experiments

Spherical treadmill

Experiments were conducted at 32°C in a closed custom arena. The spherical treadmill consisted of a 15mm diameter polyurethane foam sphere (FR-7120 foam, General Plastics) floating on an air-column. The sphere was coated with two layers of classic wood glue (Ponal, 25% in water) and then a random non-uniform pattern was drawn using two layers of acrylic black paint (Black 3.0, Culture Hustle). All coats of paint were allowed to dry overnight. The odor delivery system was similar to the one described above for *in vivo* calcium imaging experiments, but with a differing airflow rate controlled by Alicat Scientific MFCs. Continuous clean airflow was 90 mL/min and both the odor and balancer airflows were 10 mL/min. Videos were acquired with a XIMEA xiQ video camera, placed 10cm from the treadmill. The treadmill ball was illuminated by a panel of 940nm LEDs (Solarox) and an extra LED on the air-column was visible in the video and turned on simultaneously to the odor stimulus to trigger the data acquisition.

For experiments, 9-10 days old female flies were cold anesthetized and secured to a needle at their thorax on the dorsal side using a UV-hardening glue (Bondic) and positioned on the sphere with the help of a 3D micromanipulator. Before starting to record, flies were acclimatized to walking on the sphere for 10-15 minutes with no stimulus being presented. Subsequently, video recording and the odor stimulation were started. Videos were acquired using the XIMEA CamTool software: the exposure was set to 10,725ms, the gain to 2.6Db and the framerate to 80fps. The odor stimulation was controlled through MATLAB by an ARDUINO UNO Rev3 and consisted of at least 19 repetitions of 5s long odor stimuli and 20s-long interval without odor.

Fly moving speed was calculated a posteriori from the video recordings using the open-source software library FicTrac (Moore et al., 2014). For this analysis, regions of interest (ROIs), ignored regions and the transformation from the camera's frame of reference to the animal's coordinate frame were defined with the help of a configuration utility provided in FicTrac. The transformation was only calculated once at the start of experiments, since the position of the camera was never altered, but the ROIs and the ignored regions were updated for each recording. After running FicTrac, an output file was generated containing the output data, which includes rotation and speed of the animal for each frame in the video. The video recordings were also analyzed in MATLAB in order to extract the timepoints where the air-column LED was on, which corresponded to the odor stimulus being presented to the fly.

Finally, the output data from Fictrac and the timepoints obtained from the video were analyzed in MATLAB so that the moving speed during and outside odor presentation could be quantified. Flies that had a basal walking speed lower than 2mm/s were discarded.

Free-walking assay

Arena design:

A free walking area was contained in a thermally controlled black box (100x45cmx45cm) shielded from room light, fully closed with a frontal door, and equipped with a heating system and thermostat (H-TRONIC GmbH, Product ID: 1114430). The box is heated up by an air stream created by a fan (at the base of the box) and homogeneously distributed a diffuser. A blue LED stripe (470nm, Paulmann Licht GmbH, Product ID: 78979) was positioned around the walking arena to ensure stable illumination during experiments. Videos were recorded with a Basler Camera (Basler acA2040-90um) placed on the ceiling of the box and equipped with f12mm lens (Basler C10-1214-2M-S), using Pylon viewer (64-Bit, 6.3.0.10295).

The walking arena was 40.2 cm diameter and 2 cm height and composed of four stacked layers and three overlapping plates (glass or plexiglass). The bottom layer contained six holes, arranged at the corners of a hexagon, where 1.5mL glass vials (Fisherbrand 11565874) containing the test odor can be screwed in. On topo of this a Teflon® coated porous sheet (FIBERFLON GmbH & Co. KG, Product ID: 408.07 P) provides a walking surface for the flies hiding the door location. The mid arena layer consists in a sloped (at 11°, 5 cm length) ring that defines the accessible area. To sealing the walking arena, we used a glass plate coated with Sigmacote® (Sigma-Aldrich Co.) to prevent fly walking upside-down. This behavioral setup was built by the workshop of the Biology Department at Johannes Gutenberg Universität Mainz.

Experimental protocol:

We tested female flies developed at 18°C or 25°C, 5-7 days post eclosion. One hour before the experiment, flies were transferred into a vial with only a small piece of filter paper soaked in water and kept at room temperature. For experiments carried at 32°C, the fly vials were incubated for 15min in a 32°C water bath.

To create an odor gradient inside the arena, five minutes before the start of each experiment, a 1.5ml glass vial containing 1mL of test odor was placed in one of the six possible odor positions in the behavioral setup. For each trial, a fresh odor vial was used, and the position was pseudo-randomized. Each trial consisted of 10-15 female flies exposed to either apple cider vinegar (10^{-2} in MilliQ water), 2-butanone (10^{-2} in mineral oil), or tested with empty vials. Flies were gently pushed inside the arena using a custom fly transfer tube and the recording was immediately started. All experimental videos were recorded at 20 fps for 15 minutes and saved in mp4 format. At the end of each trial, the flies were removed and discarded. The initial condition was restored by removing the odor vial and the cover glass plate, replacing the Teflon® sheet with a clean one, and letting the whole system ventilate for 5 minutes.

Video processing and analysis

All required steps to pre-process the raw videos were done using the Python 3.9.12 distribution ANACONDA (Version 4.13.0). Scripts were written using Virtual Studio Code (Version 1.81.1). Recorded mp4 videos were processed and video tracked with the software TRex (Version 1.1.8_3) (Walter & Couzin, 2021). Fly trajectories were rotate to account for randomized odor position. The output files were analyzed using custom Python and MATLAB scripts. A threshold of 5cm was chosen to determine if the fly had located the odor source, variations of this threshold do not alter the results.

EM analysis

We used the Hemibrain dataset (hemibrain:v.1.2.1) (Xu et al., 2020). For Fig.1F, we considered all synapses from the or42b-ORNs of the left and right antenna within the DM1 glomerulus of the right hemisphere, which were selected by clustering the synapses bases on their 3d coordinates. The analysis was restricted to synapses of the right hemisphere, as postsynaptic partners are fully reconstructed only on this side. We calculated the number of synapses between each individual ORN and each individual post-synaptic neuron. Connections with less than 3 synapses from a single ORN were discarded. Moreover, postsynaptic neurons that received less than 10 total synapses were discarded. The same procedure was used for DL1 and DL5 for Fig.2E-F. The percentages of LNs and mPNs are lower bounds, as calculated from the available annotations.

Deriving synaptic scaling at different temperatures from a growth law with fractional power

To model ontogenetic growth, we follow the same approach of (Gillooly et al., 2002). We assume that growth scales as the 3/4 power of the mass (see discussion in the main text and (West et al., 1999)) following the equation:

$$\frac{dm}{dt} = am^{\frac{3}{4}}\left[1 - (\frac{m}{M})^{\frac{1}{4}}\right] \qquad (1)$$

where *M* is the asymptotic mass and *a* is proportional to metabolic rate:

$$a = \frac{B_0 m_c}{E_c} \qquad (2)$$

with m_c the cell mass, E_c the energy per cell and B_0 is the normalization factor of the metabolic rate $B = B_0 m^{\frac{3}{4}}$ that scales proportionally to the Boltzmann factor: $B_0 \propto e^{-\frac{E}{KT_k}}$ (T_k is the temperature in Kelvin and K the Boltzmann constant). Therefore $a \propto e^{-\frac{E}{KT_k}}$. Following (Gillooly et al., 2002) with calculate *a* with respect to reference temperature (the absolute zero T_a = 273*K*), and replacing $T = T_k - T_a$, we obtain:

$$a = a(T,E) = a(T_a,E)e^{\frac{E}{KT_a^2}\left(\frac{T}{1+\frac{T}{T_a}}\right)} \approx a(T_a,E)e^{\frac{E}{KT_a^2}T} \qquad (3)$$

The last approximation takes in account the fact that the relevant temperatures do not exceed 32°C, therefore T/T_a is at most 0.1. This approximation leads to an error of about 10% on the exponential fits, but the quality of the model prediction remains unchanged. We keep the approximation for simplicity in the following calculations.

To find the relationship between developmental time and temperature, we integrate the growth equation (1) for $m << M$ (but see below):

$$\int_0^{m(t)} m^{-\frac{3}{4}}dm = \int_0^t a(T,E)dt \Longrightarrow 4m^{\frac{1}{4}} = a(T,E)t \qquad (4)$$

Equations (3) and (4) lead to the exponential relationship between developmental time t and temperature T proposed by (Gillooly et al., 2002):

$$t = \frac{4m^{\frac{1}{4}}}{a(T_a,E)}e^{-\frac{E}{KT_a^2}T} \qquad (5)$$

We calculate the fold change with respect to a reference temperature $T_0 = 25^oC$ by assuming that development results in the same final mass:

$$\frac{t}{t_0} = e^{-\frac{E}{KT_a^2}(T-T_0)} = e^{-\alpha(T-T_0)} \quad (6)$$

with $\alpha = \frac{E}{KT_a^2}$. We use equation (5) to fit developmental times in Fig. 6I. This result remains the same if we use the general solution of equation (1) from (Gillooly et al., 2002)(relaxing the assumption $m << M$) or if we integrate it from $m(0) = m_i$ instead of $m(0) = 0$.

We now assume that developmental time follows the exponential relationship in equation (6), while the wiring of the neural circuit is constrained by a different reaction rate with $E' < E$. In modeling the growth of the neural system, we use *n* instead of the mass *m*, which can be intended as number of synapses, synaptic partners, or axonal branching. *n* follows a similar equation as (5) leading to:

$$\frac{t}{t_0} = (\frac{n}{n_0})^{\frac{1}{4}} e^{-\frac{E'}{KT_a^2}(T-T_0)} \quad (7)$$

This results from an initial condition $n(0) = 0$, which is reasonable given the major pruning and re-growth of axons that happens during metamorphosis. Using equation (6) and (7):

$$\frac{n}{n_0} = e^{-4\frac{E-E'}{KT_a^2}(T-T_0)} \quad (8)$$

where we define $\beta = 4\frac{E-E'}{KT_a^2} = 4\frac{\Delta E}{KT_a^2}$. If $\Delta E = 0$ then there should be no change in the number of synaptic partners. Also note that β can be larger than α ($\Longrightarrow E > \frac{4}{3}E'$) or smaller than α ($\Longrightarrow E' < E < \frac{4}{3}E'$). We use equation (8) to fit fold changes in number of synaptic partners in Fig. 6G.

To calculate developmental time of flies on temperature cycles with max and min temperatures T_1 and T_2. Here we simplify the cycling temperature protocol to step changes such that the final mass on temperature cycles results from development that occurs half of the time at T_1 and half at T_2:

$$\int_0^{m(\tilde{t})} m^{-\frac{3}{4}} dm = \int_0^{\frac{\tilde{t}}{2}} a(T_1, E)dt + \int_0^{\frac{\tilde{t}}{2}} a(T_2, E)dt \quad (9)$$

$$\Longrightarrow m^{\frac{1}{4}} = \frac{\tilde{t}}{8}\left[a(T_1, E) + a(T_2, E)\right] \quad (10)$$

Here $\tilde{t}$ indicates the developmental time on temperature cycles. Assuming an equal final mass, the fold change with respect to a fix temperature $\bar{T}$ is:

$$\frac{\tilde{t}}{\bar{t}} = 2\frac{a(\bar{T}, E)}{a(T_1, E) + a(T_2, E)} = 2\frac{1}{e^{-\alpha(\bar{T}-T_1)} + e^{-\alpha(\bar{T}-T_2)}} \quad (11)$$

To calculate the fold change in synaptic connectivity, we use the same logic as before to derive:

$$(\frac{\tilde{n}}{\bar{n}})^{\frac{1}{4}} = \frac{1}{2}\frac{\tilde{t}}{\bar{t}}\frac{a(T_1, E') + a(T_2, E'))}{a(\bar{T}, E')} \quad (12)$$

And using equation (11):

$$\frac{\tilde{n}}{\bar{n}} = e^{\beta\bar{T}}\left(\frac{e^{\gamma T_1} + e^{\gamma T_2}}{e^{\alpha T_1} + e^{\alpha T_2}}\right)^4 \quad (13)$$

with $\gamma = \frac{E'}{KT_a^2} = \alpha - \frac{\beta}{4}$. We use equation (13) to predict the number of synaptic partners in flies developed on periodic temperature cycles in Fig. 6L. The solutions (11) and (13) further

simplify, if we take the mean temperature as the reference temperature $\bar{T} = \frac{T_1+T_2}{2}$ and $\Delta T = \frac{T_2-T_1}{2}$ that is:

$$\frac{\tilde{t}}{\bar{t}} = \frac{1}{\cosh(\alpha \Delta T)} \tag{14}$$

and

$$\frac{\tilde{n}}{\bar{n}} = \left(\frac{\cosh(\gamma \Delta T)}{\cosh(\alpha \Delta T)}\right)^4 \tag{15}$$

which show that the fold change in developmental time and connectivity scale inversely with the amplitude of the temperature cycles (as $\gamma < \alpha$).

Gillooly, J. F., Charnov, E. L., West, G. B., Savage, V. M., & Brown, J. H. (2002). Effects of size and temperature on developmental time. *Nature*, *417*(6884), 70–73. https://doi.org/10.1038/417070A

Gorur-Shandilya, S., Demir, M., Long, J., Clark, D. A., & Emonet, T. (2017). Olfactory receptor neurons use gain control and complementary kinetics to encode intermittent odorant stimuli. *ELife*, *6*, e27670. https://doi.org/10.7554/eLife.27670

Haase, R. (2021). Image Processing Filters for Grids of Cells Analogous to Filters Processing Grids of Pixels. *Frontiers in Computer Science*, *3*, 774396. https://doi.org/10.3389/FCOMP.2021.774396/BIBTEX

Martelli, C., Carlson, J. R., & Emonet, T. (2013). Intensity invariant dynamics and odor-specific latencies in olfactory receptor neuron response. *Journal of Neuroscience*, *33*(15). https://doi.org/10.1523/JNEUROSCI.0426-12.2013

Martelli, C., & Fiala, A. (2019). Slow presynaptic mechanisms that mediate adaptation in the olfactory pathway of Drosophila. *ELife*, *8*. https://doi.org/10.7554/eLife.43735

Moore, R. J. D., Taylor, G. J., Paulk, A. C., Pearson, T., van Swinderen, B., & Srinivasan, M. V. (2014). FicTrac: a visual method for tracking spherical motion and generating fictive animal paths. *Journal of Neuroscience Methods*, *225*, 106–119. https://doi.org/10.1016/J.JNEUMETH.2014.01.010

Walter, T., & Couzin, I. D. (2021). Trex, a fast multi-animal tracking system with markerless identi cation, and 2d estimation of posture and visual elds. *ELife*, *10*, 1–73. https://doi.org/10.7554/ELIFE.64000

West, G. B., Brown, J. H., & Enquist, B. J. (1999). The fourth dimension of life: fractal geometry and allometric scaling of organisms. *Science (New York, N.Y.)*, *284*(5420), 1677–1679. https://doi.org/10.1126/SCIENCE.284.5420.1677

Xu, C. S., Januszewski, M., Lu, Z., Takemura, S., Hayworth, K. J., Huang, G., Shinomiya, K., Maitin-Shepard, J., Ackerman, D., Berg, S., Blakely, T., Bogovic, J., Clements, J., Dolafi, T., Hubbard, P., Kainmueller, D., Katz, W., Kawase, T., Khairy, K. A., … Plaza, S. M. (2020). A Connectome of the Adult Drosophila Central Brain. *BioRxiv*, 2020.01.21.911859. https://doi.org/10.1101/2020.01.21.911859